Politecnico di Torino

Master Degree in Environmental and Land Engineering
Climate Change

Geophysical characterization of an artificial water basin for seepage detection

Supervisor:

Professor Chiara Colombero

Candidate:

Mahsa Hosseinian Fard

July 2024

Contents

1 INTRODUCTION 8

1.1 Why studying man-made water basins in Alpine areas? 8

1.2 The importance of geophysical investigations in site characterization 9

1.3 Aim 10

1.4 Expected results 10

2 Test site and geophysical data acquisition 12

2.1 Test site 12

2.1.1 Location and general information: 12

2.2 Geophysical Data Acquisition 13

2.2.1 Electrical Resistivity Tomography 13

2.2.2 Seismic refraction tomography and SW analysis 14

3 Materials and Methods 15

3.1 Electrical Resistivity Tomography (ERT) 15

3.1.1 Historical Development 15

3.1.2 Definition 17

3.1.3 Electrode Configuration 17

3.1.4 Basic Principles of Electric Resistivity Method 18

3.1.5 Data Processing 19

3.1.6 Data interpretation 20

3.2 Seismic Methods in Seepage Detection 21

3.2.1 Seismic refraction tomography 21

3.2.2 Surface wave analysis 27

3.2.3 Mechanical parameters 30

4 Results 31

4.1 Electrical Resistivity Tomography Interpretation 31

4.1.1 Line ERT1 31

4.1.2 Line ERT2 32

4.2 Seismic Refraction Tomography Interpretation 34

4.2.1 Line S1 34

4.2.2 Line S2 37

4.3 Surface Wave Analysis 39

4.3.1 Dispersion Curves 39

4.3.2 Mechanical Parameters 42

4.3.3 Results Comparison 47

5 Conclusion 50

References......52

List of Figures

Figure 1: Site location map showing the study area as captured from Google Earth. 12
Figure 2: The two Electrode/Seismic arrays on the banks of the Cime Bianche basin. 13
Figure 3: Diagram showing Schlumberger set up for electric resistivity. 16
Figure 4: Wenner-Schlumberger, and dipole-dipole configuration arrays. C1 and C2 are the current electrodes, P1 and P2 are the potential electrodes and K is the configuration factor which depends on the electrodes spacing (modified after Loke et al., 2013). 18
Figure 5: ResIPy framework representation. 20
Figure 6: Reflection and refraction. Simple refraction occurs at P, critical refraction at B. 23
Figure 7: Occurrence of refraction in case of oblique incidence. (A) Normal incidence, no refraction, (B) Oblique incidence, from medium M1 to medium M2 (C) Incidence direction reversed. The velocities of the two media are V1 and V2, where V1 < V2. 24
Figure 8: Schematic first arrival times picking of seismic waves from the recorded data. 25
Figure 9: Schematic framework of pyGIMLi. 26
Figure 10: Schematic representation of surface waves. 27
Figure 11: Creating mask for each spectra to achieve dispersion curve. 29
Figure 12: 2-D Inversion results of (ERT1) survey. (a) Dipole-Dipole (b) Wenner- Schlumberger array configuration. 31
Figure 13: 2-D Inversion results of (ERT2) survey. (a) Dipole-Dipole (b) Wenner- Schlumberger array configuration. 32
Figure 14: Manually-picked first arrival travel times of seismic refraction tomography for line S1. 34
Figure 15: a) P-wave velocity model mesh grid. b) Ray coverage and tracing plot related to seismic line S1. 35
Figure 16: final P-wave velocity model for line S1. 36
Figure 17: Manually-picked first arrival travel times of seismic refraction tomography for line S2. 37
Figure 18: a) P-wave velocity model mesh grid. b) Ray coverage and tracing plot. c) final P-wave velocity model related to seismic line S2. 38
Figure 19: Final dispersion curve of Rayleigh wave velocity for a) line S1 and b) line S2. 39
Figure 20: a)The results of fitting process between experimental and theoretical dispersion curves. b) The simulation misfit graph. 40
Figure 21: The final shear wave velocity model for seismic line S1 and S2. 41
Figure 22: P-wave velocity model and interpolated Shear wave velocity model for seismic lineS1 plotted on (a): mesh elements having coverage > 1 and (b): central points of all the mesh elements (interpolated where data coverage is not available). 43
Figure 23: P-wave velocity model and interpolated Shear wave velocity model for seismic lineS2 based on (a): ray-coverage mode and (b): mesh-grid mode. 44
Figure 24: Mechanical parameters mesh-grid for line S1 in a) Ray-coverage b) Interpolation mode. 45
Figure 25: Mechanical parameters mesh-grid for line S2 in a) Ray-coverage b) Interpolation mode. 46
Figure 26: Comparison between: a)ERT investigation and b)mechanical parameters modelling results for line S1. 47
Figure 27: Comparison between: a)ERT investigation and b)mechanical parameters modelling results for line S2. 48

List of Tables

Table 1: Array information for ERT1 and ERT2 electrode lines. 14
Table 2: Array information for S1 and S2 seismic lines. 14
Table 3: Total number of iterations and final misfit (in percentage) of ERT inversion results. 33

Abstract

This thesis investigates the structural integrity and potential seepage within the embankments of an artificial water basin in the alpine region, specifically designed to support snowmaking for a ski resort. The study utilizes electrical resistivity tomography (ERT), seismic refraction and surface wave analysis to process two survey lines along the embankments. The geophysical data acquisition was carried out in the framework of the spoke “Digital and sustainable mountain” of the project NODES, funded by the National Recovery and Resilience Plan.

The ERT results reveal varying saturation levels within the embankment materials, identifying a thin surface layer with high resistivity, indicative of unsaturation, followed by a deeper layer with potential water content. Notably, a high resistivity anomaly near the drainage system suggests the presence of concrete structures or large boulders. A significant anomaly indicating possible seepage was detected along the same line. Seismic data provided estimates of the mechanical properties of the materials, showing reduced shear modulus and Young's modulus in areas with identified anomalies, confirming potential weak spots and saturation zones.

In comparison, the second line exhibited more homogeneous material with fewer resistivity anomalies and less significant mechanical property variations. The integrated geophysical approach proves effective in detecting potential leakage and assessing the embankment's condition, offering valuable insights for the maintenance and safety of artificial water basins in alpine environments. The study underscores the importance of combining geophysical techniques for comprehensive site characterization and risk mitigation in similar infrastructures.

Acknowledgments

I sincerely thank all those who have given me their support. First and foremost, I extend my heartfelt thanks to my professor, Chiara Colombero. Your invaluable expertise, insightful guidance, and unwavering support have been instrumental in the successful completion of this thesis. Your encouragement and constructive feedback have not only enhanced the quality of my work but also enriched my academic experience. I am deeply grateful for the opportunities and knowledge you have provided.

I would also like to thank my partner in crime, Sina. Your constant support, patience, and understanding have been my source of strength during this challenging journey. Your belief in me has kept me motivated, and your assistance and encouragement have been crucial in helping me stay focused and determined. I am incredibly fortunate to have you by my side.

Finally, I extend my appreciation to all those who have contributed to this thesis, directly or indirectly. Your support and encouragement have been greatly valued.

Thank you all for your significant contributions to this work.

1 INTRODUCTION

1.1 Why studying man-made water basins in Alpine areas?

Alpine ski resorts are iconic for their snowy landscapes and robust winter tourism, attracting millions of visitors annually. However, maintaining these resorts, particularly in the face of increasingly unpredictable snowfall due to climate change, relies heavily on the infrastructure of man-made water basins. These basins, or artificial reservoirs, are crucial for storing water needed for snowmaking, which has become essential for ensuring consistent ski conditions and extending the ski season.

Snowmaking involves creating artificial snow by spraying water into the cold air, where it crystallizes and falls as snow. This process is dependent on a reliable water supply, typically sourced from man-made water basins. These basins provide the necessary volumes of water during periods of low natural snowfall, ensuring that resorts can maintain high-quality slopes and meet the demands of winter sports enthusiasts (Steiger & Mayer, 2008).

The importance of these water basins extends beyond snowmaking. They help stabilize the local economy by enabling resorts to attract visitors even in seasons with poor natural snow, thereby supporting jobs and businesses dependent on winter tourism (Rixen et al., 2011). Additionally, while the construction of these basins raises environmental concerns, such as impacts on local hydrology and ecosystems, they are critical for the operational viability of ski resorts (Hanzer et al., 2018).

Case studies from European ski resorts demonstrate how effective water basin systems can ensure operational stability and economic sustainability. For instance, in the Austrian Alps, ski resorts use these basins to guarantee snow cover and extend their ski seasons, making them more resilient to climatic changes (Fischer et al., 2012).

In summary, man-made water basins are indispensable for the sustainability and success of alpine ski resorts. They provide the necessary resources for snowmaking, support local economies, and help mitigate the impacts of climate variability.

1.2 The importance of geophysical investigations in site characterization

Utilizing geophysical methods offers a complete and budget-friendly approach to assessing the effectiveness of dams and linear infrastructure non-intrusively complementary to other surveying techniques. They can be applied across large areas or volumes of the sub-surface. It is essential to conduct thorough assessments of embankment dams and water basins to ensure their internal structures and integrity. Most dam inspections today, whether visual or instrumental, focus primarily on identifying external indicators of potential issues, such as cracks, movements, or increased seepage flow. Unfortunately, these inspections might not detect problems caused by internal processes until they have already progressed. While more detailed studies, such as geotechnical investigations, can be carried out, these methods are often intrusive and costly, particularly when applied to an entire site. It is encouraging to observe that geophysical methods are increasingly playing a significant role in the assessment of linear anthropogenic infrastructures globally, similar to traditional geotechnical investigation methods. Both geotechnical and geophysical methods share the same objectives: to characterize the soil, rock, and groundwater at potential dam sites and to examine anomalies in existing dams. These assessments focus on properties such as shear modulus, bulk density, porosity, lithology, fracturing patterns, weathering, fracture orientation, depth to bedrock, and fault location. Notably, some geophysical methods offer advantages over traditional geotechnical methods. They can monitor water seepage and detect the formation of voids or sinkholes, often at a lower cost. Techniques such as Electromagnetic Profiling, Electrical Resistivity Tomography, Ground Penetrating Radar, Seismic Methods, and Temperature Measurements are among the geophysical methods used. The selection of specific methods or their combinations depends on various factors, but it is widely acknowledged that these techniques are now well-established for these applications, with many other methods gaining popularity. (Adamo, et al.2020). Understanding what's beneath the ground is essential for the success of many construction and environmental projects. Geophysical investigations are invaluable for this purpose, offering non-invasive and cost-effective methods to explore subsurface conditions. Techniques like seismic refraction, electrical resistivity tomography (ERT), and ground-penetrating radar (GPR) provide detailed insights into subsurface features. These insights help engineers and geologists make informed decisions about site development and risk mitigation, ensuring the stability and safety of structures such as buildings, dams, and embankments (Reynolds, 2011). These methods bring

significant environmental and economic benefits. By reducing the need for extensive drilling and excavation, geophysical investigations minimize environmental disruption and lower project costs. They optimize site exploration, focusing efforts on critical areas and thus enhancing the overall efficiency and sustainability of projects (Kearey, et al. 2013). For example, in constructing earth dams or assessing existing structures, these techniques can detect weaknesses, identify seepage paths, and monitor structural integrity over time (Butler et al., 2012). Geophysical methods have diverse applications across various fields. In environmental assessments, they can map contamination plumes or assess landfill integrity. In civil engineering, they support the design and construction of foundations, tunnels, and other infrastructure. Even in archaeology, these techniques allow for the exploration of buried artifacts without disturbing the site. This versatility underscores the crucial role of geophysical investigations in modern site characterization, making them indispensable for safe, efficient, and sustainable project development (Schrott & Sass, 2008).

1.3 Aim

The focus of this thesis is to explore and assess the structural integrity of a man-made water basin nestled in the alpine terrain, specifically designed to supply water for snowmaking at a ski resort. In these picturesque but demanding environments, ensuring the reliability of such reservoirs is crucial. This study aims to determine whether the basin's embankments are secure or if there are hidden leaks that could undermine its effectiveness and the resort's operations. By employing advanced geophysical and geotechnical techniques, we will thoroughly investigate the embankments to identify any subtle seepage or potential weak spots. The goal is to provide a clear and comprehensive understanding of the basin's health, ensuring it can continue to support the creation of pristine snow, vital for the resort's success and the enjoyment of its visitors. This investigation not only seeks to protect the infrastructure but also to sustain the vibrant winter tourism that brings life to these stunning alpine landscapes.

1.4 Expected results

Geophysical investigation techniques such as electrical resistivity tomography (ERT) and seismic refraction and surface wave analyses can help to identify anomalies within the embankments, such as areas of increased moisture content or variations in subsurface

composition. By correlating these findings with the mechanical properties of the embankments, potential leaks, seepage pathways, or structural weaknesses can be pinpointed. This knowledge would enable informed decision-making to address any identified concerns and safeguard the effectiveness and longevity of the water basin for supporting snow production at the ski resort.

2 Test site and geophysical data acquisition

2.1 Test site

2.1.1 Location and general information:

The locality of Cime Bianche is situated in the Aosta Valley region, in the Italian Western Alps (Figure 1). This area is part of the Monte Rosa massif and lies close to the famous ski resorts of Cervinia and Valtournenche[1]. The region is renowned for its stunning alpine landscapes and unique ecosystems that have been preserved since the last ice age. The area is also a hotspot for alpine tourism, offering hiking paths, ski lifts, and panoramic views of the Matterhorn. The resort offers a variety of ski runs and modern amenities to support winter tourism. Cime Bianche basin, particularly, is constructed with the aim of ensuring optimal skiing conditions throughout the season by storing water needed for snowmaking.

Figure 1: Site location map showing the study area as captured from Google Earth.

The area provides an essential habitat for alpine flora and fauna, contributing to its designation as a biotope of outstanding natural interest and a Special Protection Area within the Natura 2000 network (Pogliotti et al., 2015). The Cime Bianche basin is located at high elevation (2,985 m). There is no information about the materials and construction setup of the basin embankments. However, it is assumed that the basin was excavated inside the shallow deposits of the site and the excavated material was compacted on the sides to create

[1] https://eniscuola.eni.com/en-IT/articles/2020/ecosystems/the-last-wild-valley-in-defence-of-the-cime-bianche.html

the embankments. An impermeable membrane was then laid on the bottom of the lake. A drainage system is present of the western embankment, build of a concrete structure and big rock boulders.

2.2 Geophysical Data Acquisition

2.2.1 Electrical Resistivity Tomography

A series of electrodes are placed into the ground along two predefined lines (ERT1 and ERT2) as shown in (Figure 2) which are located in the down side of the natural slope.

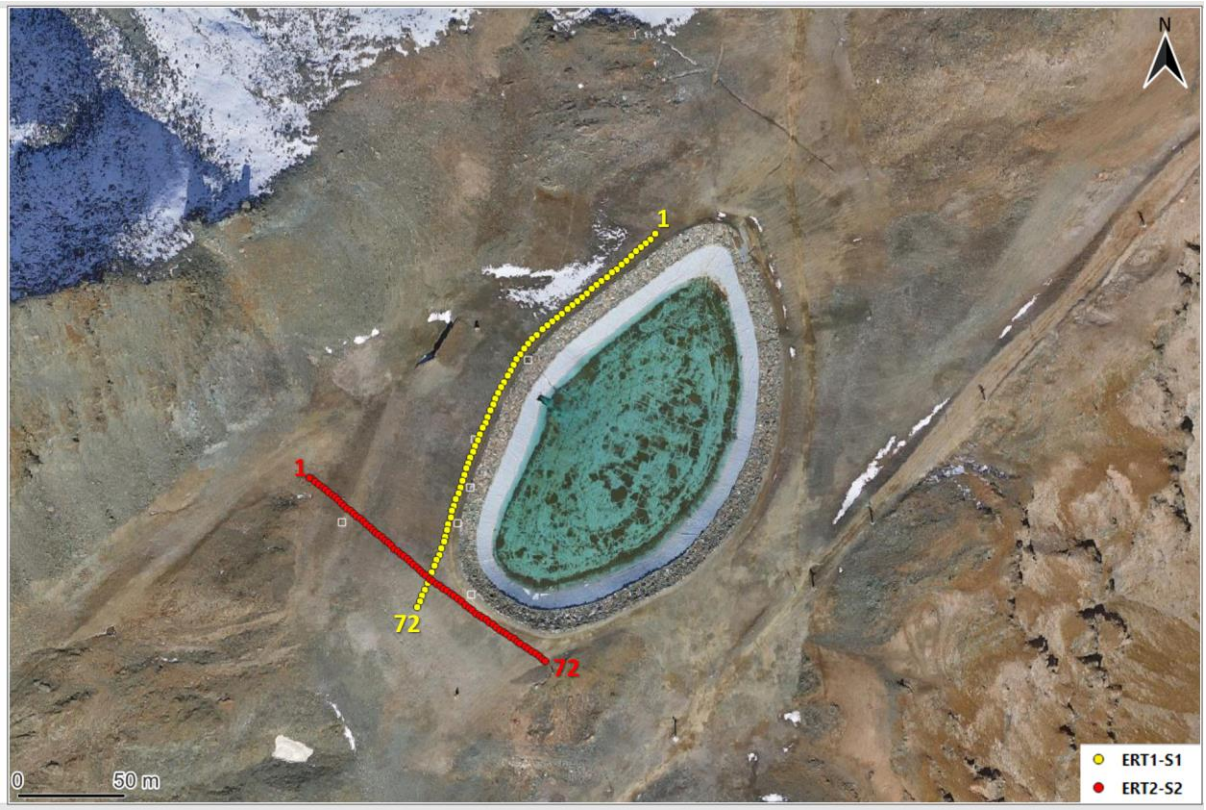

Figure 2: The two Electrode/Seismic arrays on the banks of the Cime Bianche basin.

During the acquisition, these electrodes are arranged in specific configurations, known as arrays. The two configurations which are used for each array in this study include the Wenner-Schlumberger, and dipole-dipole arrays, each suited to different depths and resolutions. The spacing between electrodes is chosen based on the desired depth of investigation and the resolution required. Closer spacing provides higher resolution but shallower penetration,

while wider spacing allows for deeper investigation at the cost of resolution. The array information can be seen in below table (Table 1).

Table 1: Array information for ERT1 and ERT2 electrode lines.

Array	Number of Electrodes	Spacing (m)	Overall Survey Length(m)
ERT1	72	3	213
ERT2	72	2	142

2.2.2 Seismic refraction tomography and SW analysis

The process starts with designing the survey, where the layout of the survey lines is planned to optimize data coverage. Next, seismographs are prepared to record seismic waves, and geophones are deployed along the survey line to detect these waves. Data collection begins with wave generation, where seismic waves are initiated at the source and propagate through the subsurface, refracting back or travelling parallel to the surface. A 8-kg sledgehammer was used as a seismic source at different locations along the lines. Geophones detect these waves and send signals to seismographs, which record the arrival times. Multiple shots are conducted along the survey line to ensure comprehensive coverage and account for subsurface variability. The seismic array location and information are similar to ERT survey as mentioned respectively in Figure 2 and Table 2.

Table 2: Array information for S1 and S2 seismic lines.

Array	Number of Geophones	Spacing (m)	Number of shots	Overall Survey Length(m)
S1	72	3	20	213
S2	72	2	21	142

3 Materials and Methods

This study utilized two geophysical techniques: Seismics and Electrical Resistivity Tomography (ERT). By combining these methods, we can significantly reduce the uncertainties that often arise when relying on a single method for interpretation. The integration of Electrical Resistivity Tomography (ERT) and seismic methods has significantly advanced geophysical investigations. ERT is highly sensitive to changes in moisture content and material type, providing detailed resistivity maps, while seismic methods are sensitive to mechanical properties and structural features, offering high-resolution images of subsurface structures. Modern advancements include simultaneous data acquisition and joint inversion algorithms, which enhance the accuracy and resolution of subsurface models. This integration is particularly beneficial in environmental monitoring, hydrogeology, and geotechnical engineering, allowing for comprehensive assessments of conditions such as contamination plumes, groundwater flow, and structural integrity of dams and embankments (Auken et al., 2015; Binley & Kemna, 2005; Chambers et al., 2002; Loke et al., 2013).

3.1 Electrical Resistivity Tomography (ERT)

3.1.1 Historical Development

Electrical geophysical methods were among the earliest used in dam assessments. The development of electrical prospecting began with Fox's exploration of natural earth currents in 1830, progressing through Schlumberger's successful application of direct currents. Today, the field includes the use of alternating currents and electromagnetic fields in addition to direct currents.

Initially, resistivity data interpretation relied on empirical methods, which are still prevalent. Other techniques have since been developed, such as transforming resistivity data into geological information through mathematical transformations, as described by Norstrand et al. in 1966. The application of resistivity data in engineering geophysics was recognized in 1928 when Crosby and Leonardon applied electrical methods to map bedrock topography at a proposed dam site on the upper Connecticut River. This instance marked the first use of these methods for engineering purposes in the United States. In this case, the bedrock consisted of high-resistivity Precambrian schist, covered by about 150 feet of glacial drift, with

a resistivity contrast of approximately 10:1. The Schlumberger method, involving vertical electrical sounding with a single quadrupole, was employed. Preliminary measurements at eight test holes before the full survey showed that five of the measurements were accurate within 5 percent, while the rest were within 20 percent accuracy (Lin et al., 2018). In electrical resistivity profiling, the distance between the voltage/potential electrodes is designated as *a*, the distances from these electrodes are *c*, and the probe's depth of penetration is *b* (Figure 3). Using the Schlumberger method, if *b* is small compared to *a* and *c*, and *c* >2*a*, the apparent resistivity value can be calculated. The Schlumberger setup for electrical resistivity is illustrated in the Figure 3.

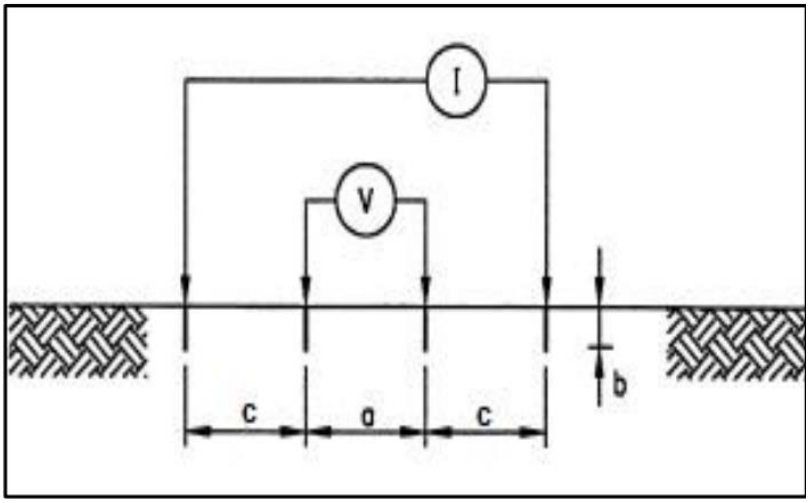

Figure 3: Diagram showing Schlumberger set up for electric resistivity.

Since 1928, geophysical methods have been incorporated into investigation programs for potential dam sites. However, the further development of geophysical applications for existing dams has largely focused on the operational phase after the dam's completion. Dams are large structures, and their internal hydraulic conditions often require monitoring before issues become apparent through simple reconnaissance methods, visual inspections, and instrumental monitoring. These traditional methods do not offer insights into the internal dynamics of the dam, and the discrete monitoring instruments provide engineering parameters with limited spatial coverage. As a result, there is an increasing demand for non-destructive geophysical techniques that can internally image dams, enabling the early detection of anomalies and facilitating prompt remedial actions. Geophysical techniques such as time domain reflectometry, refraction tomography, electrical resistivity tomography, and multichannel analysis of surface waves (MASW) have significantly advanced over the last few

decades. The application of these methods to dams has garnered considerable interest among engineers. A deeper understanding of the connections between geophysical results and their engineering significance related to dam safety and sustainability can provide engineers with more valuable information when utilizing these technologies (Adamo et al., 2020).

3.1.2 Definition

Nowadays, ERT is the most utilized electrical method which involves measuring ground resistivity by introducing a direct current into the subsurface through two current electrodes. The electrical potential difference is then recorded as a voltage with the help of two additional potential electrodes. These voltage readings are converted into apparent resistivity values. The electrode set is incrementally shifted by one electrode length laterally until the entire area is covered. Subsequently, the electrode spacing is progressively increased by one electrode to explore deeper layers. This procedure is repeated until the desired depth levels are achieved, resulting in the creation of a pseudo-section. The data acquisition is managed by software. The obtained apparent resistivities are then used to model the actual resistivity distribution of the subsurface (Reynolds, 2011; Telford et al., 1990). The effectiveness of the ERT survey depends on the electrode configuration, the spacing between electrodes, the signal-to-noise (S/N) ratio, and the inversion algorithm used. (Cardarelli & De Donno, 2019).

3.1.3 Electrode Configuration

Selecting the appropriate electrode configuration is influenced by the structure being investigated, the level of ambient noise, and the sensitivity of the resistivity meter. Common configurations for data acquisition include the Wenner, dipole-dipole, and Schlumberger arrays, among others. The Wenner array is particularly suitable for areas with high background noise due to its strong signal strength (high S/N ratio) and sensitivity to vertical resistivity changes while being less sensitive to lateral variations. This makes it highly effective for detecting horizontal structures. Conversely, the dipole-dipole array offers good data coverage and sensitivity to horizontal resistivity changes, but it tends to suffer from background noise and has a lower S/N ratio compared to the Wenner array, making it ideal for mapping vertical structures. The Schlumberger array provides moderate sensitivity to both horizontal and vertical structures, with a signal strength stronger than that of the dipole-

dipole array but weaker than the Wenner array (Loke, 2020). This survey is carried out using dipole–dipole and Wenner-Schlumberger. The Wenner-Schlumberger (WS) configuration is a widely used electrode arrangement in Electrical Resistivity Tomography (ERT) investigations. This configuration combines aspects of both the Wenner and Schlumberger arrays, providing a balance between depth penetration and lateral resolution, making it highly effective for various geophysical applications. In the context of dam and embankment investigations, it helps identify seepage paths, monitor structural integrity, and detect potential weaknesses (Soupios et al., 2007). The following figure shows these two configuration (Figure 4):

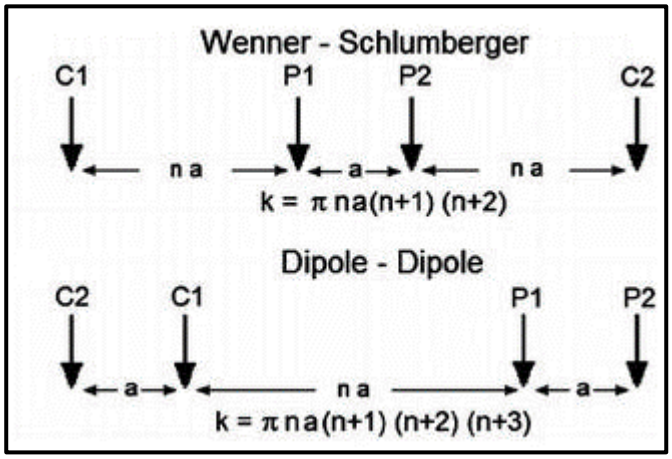

Figure 4: Wenner-Schlumberger, and dipole-dipole configuration arrays. C1 and C2 are the current electrodes, P1 and P2 are the potential electrodes and K is the configuration factor which depends on the electrodes spacing (modified after Loke et al., 2013) [2].

3.1.4 Basic Principles of Electric Resistivity Method

Electrical resistivity imaging is a commonly employed method in near-surface geophysical surveys for investigating various geological, environmental, and engineering issues, including landslides and the integrity of earth fill dams and levees. The purpose of electrical surveys is to determine the subsurface resistivity distribution by conducting measurements at the ground surface, which allows for the quantification of the true resistivity of the subsurface. This resistivity is influenced by various geological factors, such as mineral and fluid content,

[2] Development of a geophysical and geochemical methodology for, the characterization of hydrocarbon contamination of soil and groundwater - Scientific Figure on ResearchGate. Available from: https://www.researchgate.net/figure/The-different-configuration-arrays-wenner-wenner-schlumberger-pole-dipole-and_fig40_325956458

porosity, and the degree of water saturation within rocks or fill dams. For many decades, electrical resistivity surveys have been utilized in hydrogeological, mining, and geotechnical investigations of engineering structures. More recently, they have also been applied in environmental surveys and dam safety monitoring. As previously mentioned, resistivity measurements typically involve injecting an electric current into the ground using two electrodes (C1 and C2) and measuring the resulting voltage difference with two potential electrodes (P1 and P2). The resistivity (ρa) is then calculated using the current (I) and voltage (V) values, according to the formula 1:

$$\rho\alpha = k\, V / I \qquad (1)$$

where (k) is the geometric factor which depends on the configuration of the four electrodes. Resistivity is defined as R = V/I, thus the apparent resistivity value is calculated in practice by (Adamo et al.,2020):

$$\rho\alpha = k\, R \qquad (2)$$

3.1.5 Data Processing

The resistivity value calculated from Equations 1 and 2 is not the true resistivity of the subsurface but rather an "apparent" resistivity. This apparent value represents the resistivity of a hypothetical homogeneous ground that would produce the same resistance for the given electrode configuration. The relationship between apparent resistivity and true resistivity is complex. To determine the true resistivity, the measured apparent resistivity values are inverted using mathematical equations, a process that has been significantly simplified by the advent of computer programs. In this study, the obtained ERT data are inverted easily with the aid of ResIPy software. Its framework can be seen in the below figure (Figure 5).

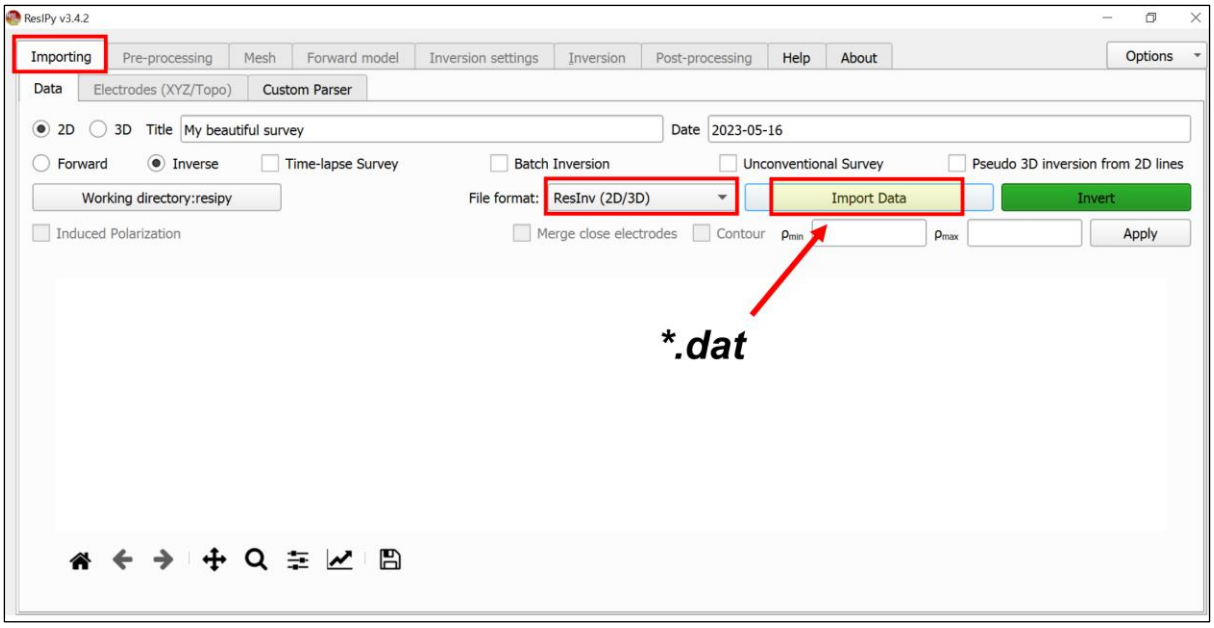

Figure 5: ResIPy framework representation.

ResIPy is an open-source software for processing, inversion, and visualization of Electrical Resistivity Tomography (ERT) data. It features an intuitive graphical user interface (GUI) that supports various data formats and allows for comprehensive data preprocessing, including filtering and geometric corrections. The inversion process aims to minimize the difference between the observed apparent resistivity data and the simulated data from the forward model. This is done iteratively, updating the subsurface model in each iteration. Coupled with a series of regularizations, it generates 2D and 3D resistivity models and offers robust tools for visualizing and interpreting these models. Additionally, ResIPy supports data export and report generation, making it a versatile tool for geophysical investigations (Blanchy et al., 2020; Nguyen & Kemna, 2020). The final product would be detailed maps, cross-sections, and 3D visualizations of the resistivity data to facilitate a better understanding of the subsurface conditions which would be interpreted later.

3.1.6 Data interpretation

Interpreting ERT diagrams for detecting water seepage involves identifying low-resistivity anomalies that signify water-saturated zones within embankments or dam structures. These low-resistivity areas, indicated by cooler colors on the diagram, suggest potential seepage paths due to the higher conductivity of water compared to surrounding materials. By

correlating these anomalies with known structural features such as cracks or weak zones, and validating them against geological and hydrological data like borehole logs and historical seepage records, one can effectively pinpoint seepage locations. Additionally, analyzing the depth and extent of these anomalies helps assess the severity of seepage, while time-lapse ERT studies can monitor changes over time and evaluate mitigation efforts (Soupios et al., 2007; Chambers et al., 2014; Loke & Barker, 1996)

3.2 Seismic Methods in Seepage Detection

The use of seismic methods for detecting seepage in embankments and dams dates back to the mid-20th century. Early efforts focused on understanding seismic wave propagation through different materials. The United States Bureau of Reclamation (USBR) conducted foundational studies in the 1950s and 1960s using seismic refraction techniques to identify subsurface anomalies that could indicate potential seepage paths (USBR, 1960). Significant advancements occurred in the 1970s and 1980s, particularly in seismic equipment and data processing techniques. Seismic reflection methods, offering higher resolution images than refraction methods, became more prevalent. These methods were employed to assess dam foundations and detect seepage zones. For instance, Lagoe et al. (1979) utilized seismic reflection to identify seepage paths in earth dams (Lagoe et al., 1979).

3.2.1 Seismic refraction tomography

The first time the seismic refraction use of an artificial source in a seismic experiment is done by Irish physicist, Robert Mallett in 1846 and in 1910, L. Mintrop use for the first-time seismic waves transmit through the earth subsurface. At the same year the scientist Mohorovicic, identified and separated P and S waves on travel-time plots and associates them with base of the crust, (the Moho discontinuity). In 1916, the method developed to locate artillery guns by measurement of recoil and in 1919 applied it to determine depths and types of subsurface formation. Seismic refraction was the first seismic technique to be used in petroleum exploration, and in the 1920's, E. V. McCollum used it in the USA. In 1925 the refraction method was well established as a tool in applied geophysics. In the early days the method was used for oil exploration and for detecting hidden salt domes. At the beginning of the 'thirties the refraction technique was also seen to be applicable to civil engineering problems. (Sjogren, Bengt, 1984). Refraction seismology is applied to a very wide range of scientific and

technical problems, from engineering site investigation surveys to large-scale experiments designed to study the structure of the entire crust or lithosphere. Refraction measurements can provide valuable velocity information for use in the interpretation of reflection surveys, and refracted arrivals recorded during land reflection surveys are used to map the weathered layer (Kearey et al., 2013) The depth of investigation depended on the size of the source and the length of the seismic spread, which needs to be 4-5 times the depth of investigation. For shallow investigation can be use in civil engineering for geotechnical work to determine the strength of a material and its composition, calculate the elastic moduli, assess the rock quality. Determine tunnels and their entrances, oil and petrol storage depots, air raid shelters, military installations, factories, mines and sewage treatment plants (Redpath, 1973).

3.2.1.1 Basic principles of seismic refraction

When a seismic wave transmitted through the earth subsurface and reaches to boundary between two different mediums (layers), some of the energy is reflected and the others refracted and transmits into the earth with a different angle (Figure 3). A seismic wave incident on an interface is partly reflected and therefore partly transmitted. In the general case where the wave is obliquely incident on the interface the transmitted wave changes direction (refracted). It will be bent either towards the normal line (normal to the interface at point of incidence) or away from that normal. The amount of bending (angle of refraction) and the sense of bending (towards or away from the normal) are governed by the velocities of the two layers separated by the interface (Snell's law). The refracted ray is bent away from the normal in case of the velocity in the medium in which the wave is refracted) is greater than that in the medium that hosts the incident wave. The bending of the refracted wave is towards the normal when the velocity of the medium, in which refraction occurs, is of lower value (Figure 6).

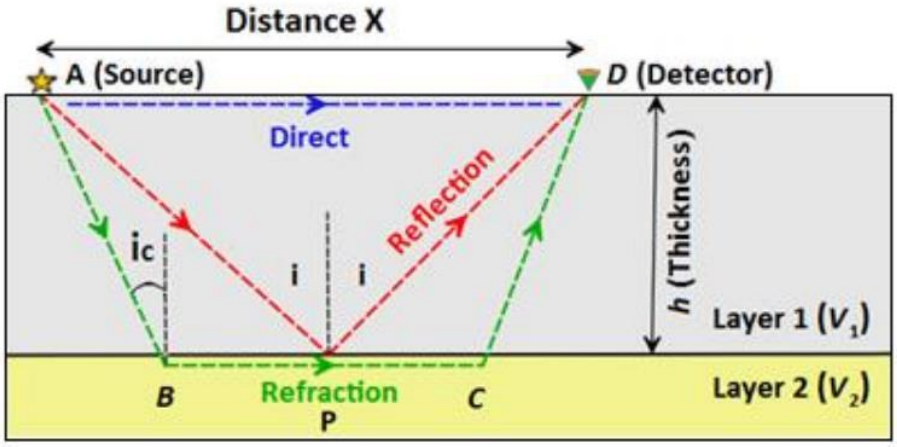

Figure 6: Reflection and refraction. Simple refraction occurs at P, critical refraction at B[3].

In essence, the phenomenon of ray bending (wave refraction) at an interface occurs only when the incidence direction is inclined to the interface. Refraction of an incident seismic wave at an interface is governed by Snell's law which states that the ratio of the sine of angle of incidence (i) to the sine of angle of refraction (r) is equal to the ratio of velocity in the first medium (in which the wave is incident) to that of the second medium (in which the wave is refracted). In reference to (Figure 7), Snell's law takes the following form:

$$\frac{sin\ i}{sin\ r} = \frac{V1}{V2} \qquad (3)$$

[3] Alsadi, Hamid & Baban, Ezzadin. (2020). Introduction to the Seismic Exploration.

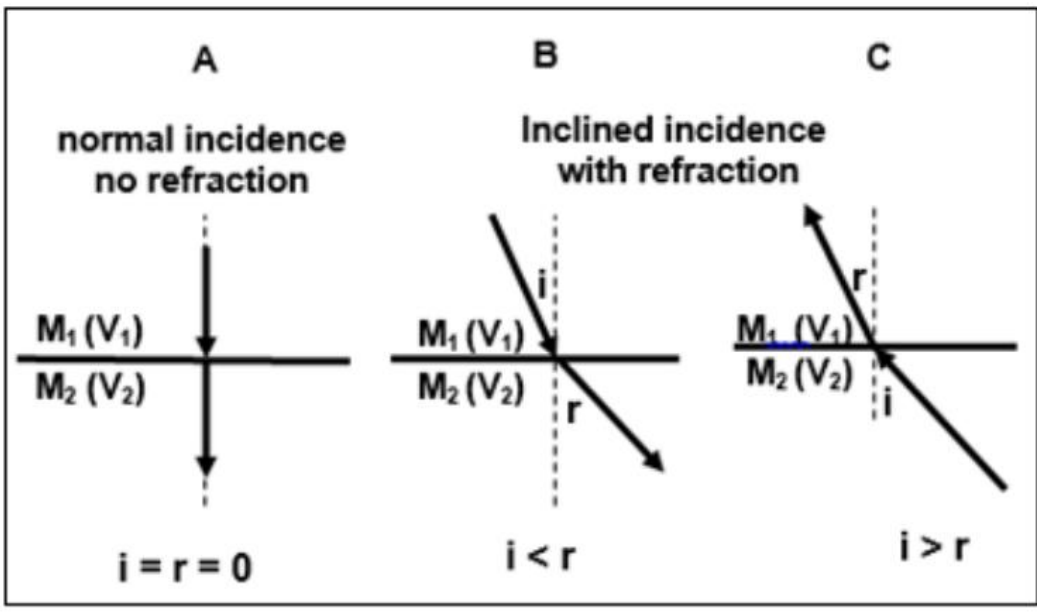

Figure 7: Occurrence of refraction in case of oblique incidence. (A) Normal incidence, no refraction, (B) Oblique incidence, from medium M1 to medium M2 (C) Incidence direction reversed. The velocities of the two media are V1 and V2, where V1 < V2[4].

3.2.1.2 Primary wave analysis

P-waves, or primary waves, are compressional seismic waves generated by earthquakes and other seismic sources, traveling faster than other seismic waves and arriving first at seismic stations. They cause particles in the material to oscillate parallel to the wave's direction of propagation, creating compressions and rarefactions. P-waves can move through solids, liquids, and gases, with speeds ranging from few hundreds of m/s in the near-surface to 5-8 km/s in the Earth's crust, depending on the medium's density and elastic properties. Detected by seismographs, P-waves provide initial data on an earthquake's location and magnitude, and their travel times are crucial for modeling the Earth's internal structure. Variations in their velocities help identify different rock types and geological features (Shearer, 1999; Lay & Wallace, 1995; Aki & Richards, 2002; Stein & Wysession, 2003).

3.2.1.3 Data processing to retrieve P-wave velocity from seismic refraction data

- **First arrival picking**: the first arrival times of seismic waves from the recorded data along lines S1 and S2 for all the available shots are accurately picked (Figure 8) . It is

[4] Alsadi, Hamid & Baban, Ezzadin. (2020). Introduction to the Seismic Exploration.

critical as it directly impacts the quality of the inversion results. This step is carried on by manual picking with the help of a Matlab code.

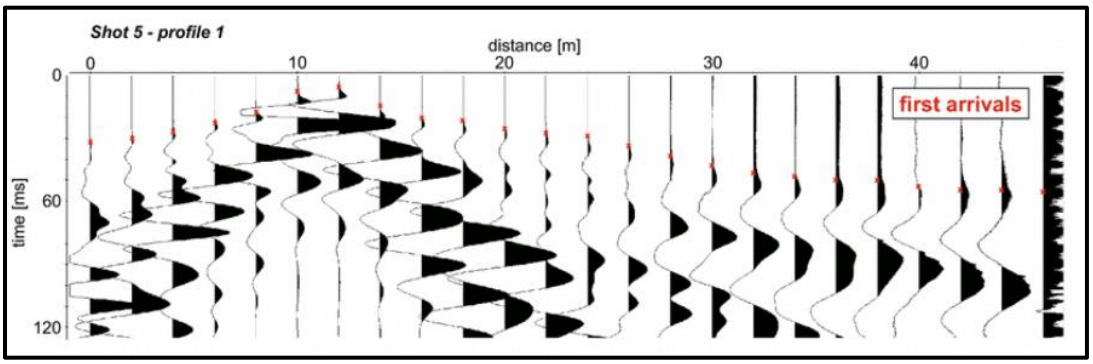

Figure 8: Schematic first arrival times picking of seismic waves from the recorded data[5].

- **Tomographic Inversion**: The picked travel time data are used inside a Python library, pyGIMLi, containing tools for modelling and inversion of geophysical data in order to retrieve the P-wave velocity model which is later needed to compute mechanical properties of the site. Figure (9) shows a default framework of pyGIMLi.

[5] Integration of seismic and sedimentological methods for analysis of Quaternary alluvial depositional systems - Scientific Figure on ResearchGate. Available from: https://www.researchgate.net/figure/Processing-steps-manual-picking-of-the-first-arrivals-red-crosses-and-travel-time_fig4_311893932

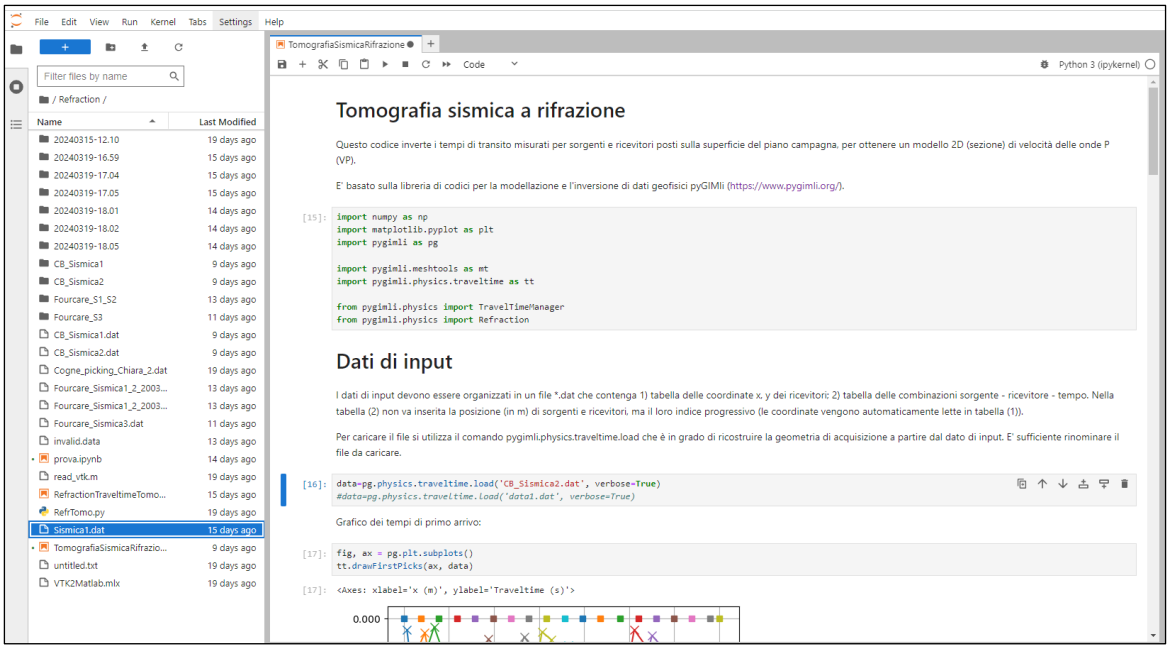

Figure 9: Schematic framework of pyGIMLi.

The basic methodology of inversion involves transforming observed travel time data into a subsurface velocity structure model. An initial velocity model, based on prior geological information, is created, and theoretical travel times are calculated. The differences between observed and calculated travel times (residuals) indicate the initial model's accuracy. The inversion process linearizes the relationship between travel times and velocity structure using the Jacobian matrix, which describes the sensitivity of travel times to velocity changes. Optimization algorithms, such as least squares inversion, adjust the model to minimize residuals iteratively. The velocity model is updated until the residuals are minimized, yielding the final P-wave velocity model. This model is validated with additional data or comparisons to known geological features. The mathematical foundation includes the eikonal equation and linearized inversion, which relate travel time changes to velocity perturbations (Aki & Richards, 2002; Menke, 1989; Nolet, 1987; Stein & Wysession, 2003).

3.2.2 Surface wave analysis

S-waves, or secondary waves, are shear seismic waves generated by earthquakes, traveling slower than P-waves and arriving second at seismic stations. They move perpendicular to the wave propagation direction, causing shearing motions in the material, which makes them more destructive than P-waves. S-waves can only travel through solids, as fluids do not support shear stress (Figure 10). Their velocity, typically up to around 3-4.5 km/s in the Earth's crust, depends on the medium's shear modulus and density. Detected by seismographs, S-waves provide critical data on the Earth's interior structure, helping to delineate solid from liquid layers. The inversion of S-wave dispersion curve, allows geophysicists to construct shear wave velocity models, enhancing the understanding of subsurface properties (Aki & Richards, 2002; Lay & Wallace, 1995; Shearer, 1999; Stein & Wysession, 2003).

The retrieval of S-wave velocity models from refraction analysis implies the use of sources and receivers able to detect the shear waves (i.e., horizontally oriented with respect to the ground surface). S-wave velocity models can be alternatively retrieved from the analysis of the surface wave content of the seismic records. As shown in Figure 10, there are two types of surface waves. Rayleigh waves are generally the focus of investigation since their velocity is very close to the one of shear waves (VR=0.92Vs).

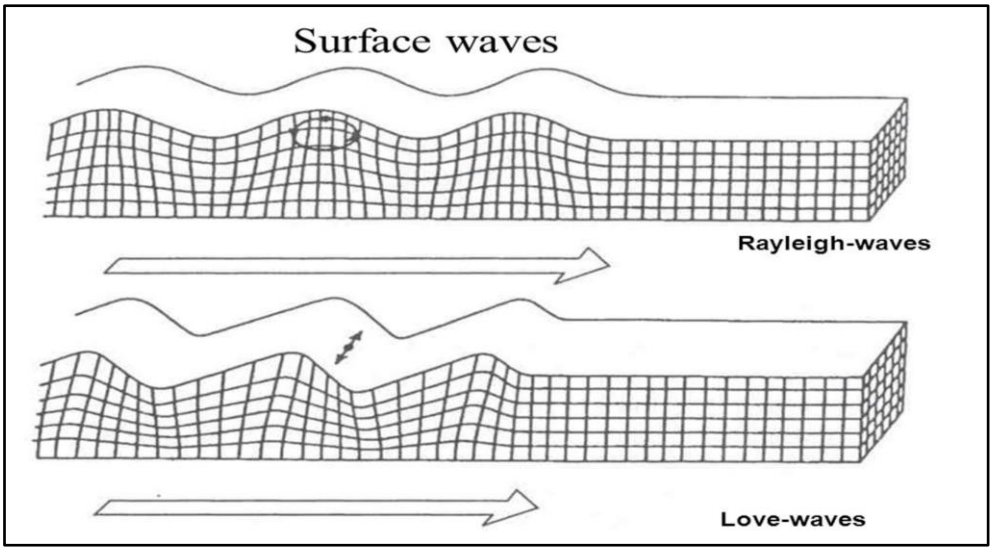

Figure 10: Schematic representation of surface waves[6].

[6] https://publications.chitkara.edu.in/note-on-surface-wave-in-fibre-reinforced-medium/

3.2.2.1 Data processing

Rayleigh waves exhibit dispersion, meaning their phase velocity varies with frequency. This property is exploited to analyse the subsurface structure. Higher frequency waves typically sample shallower depths, while lower frequencies penetrate deeper (Foti et al., 2014). There are different spectral computations that might be applied to extract dispersion curves from the raw data:

- **Fourier Transform**: Fourier transform should be applied to the travel time series to convert them from the time domain to the frequency domain(spectra).

- **Frequency-Time Analysis**: the frequency content should be analysed over time to identify how different frequencies travel at different speeds.
- **Phase Velocity Calculation**: phase velocities at various frequencies should be calculated to construct the dispersion curve (Aki & Richards, 2002).

In this study, with the help of Matlab codes, firstly frequency-phase velocity spectra relative to a moving window of a number of receivers along the spread for each source are calculated. Then in order to improve the spectra ratio, all available spectra for each window are stacked and the maxima for each frequency is automatically identified. In the next step for each spectra, a mask is created manually to contain the points in the fundamental mode area (area of lower velocities related to each frequency component) as shown in the (Figure 11). Points outside the polygon will be discarded. In this way the dispersion curves related to the fundamental mode of Rayleigh waves are extracted which would be used further for retrieving shear velocity model, through an inversion procedure.

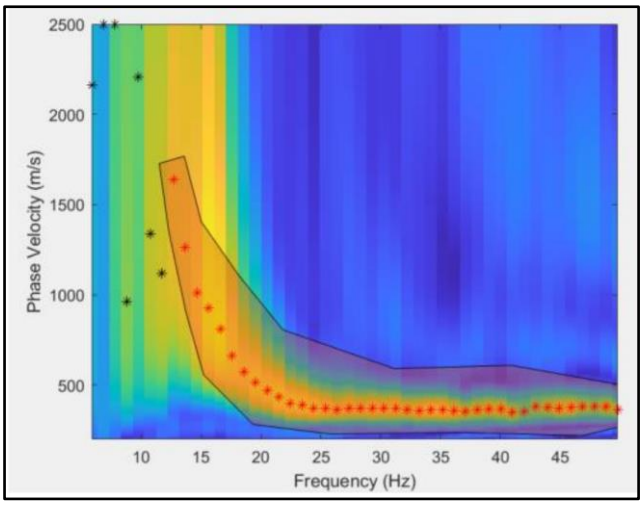

Figure 11: Creating mask for each spectra to achieve dispersion curve.

3.2.2.2 Inversion for shear velocity model

Inversion is a mathematical process used to derive subsurface properties from observed data. In this context, we invert the dispersion curves to obtain a shear velocity model (Nolet, 1987). To do this, an initial model is needed to start with. An initial shear wave velocity model is proposed based on prior knowledge or assumptions about the subsurface. This model serves as a starting point for the inversion process (Dziewonski & Anderson, 1981). The final shear velocity model provides a detailed representation of the subsurface shear wave velocities, which can be interpreted to understand geological structures, material properties, and dynamic processes within the Earth. The inversion process is described briefly below:

- **Forward Modelling**: Generate synthetic dispersion curves from the initial shear velocity model.
- **Error Minimization**: Compare synthetic dispersion curves with observed curves and minimize the error by adjusting the model parameters.
- **Iteration**: Repeat the forward modeling and error minimization steps iteratively until the model converges to an optimal solution (Herrmann, 2013).

The final shear velocity model provides a detailed representation of the subsurface shear wave velocities, which can be interpreted to understand geological structures, material properties, and dynamic processes within the Earth (Aki & Richards, 2002; Yilmaz, 2001).

3.2.3 Mechanical parameters

After retrieving a P-wave and S-wave subsurface section, the last step of this thesis is dedicated to computing the mechanical properties of the underlying layers of seismic lines (S1) and (S2) . This process consists of calculating the Poisson's ratio, Young's modulus and Shear modulus in order to see how mechanical parameters are variable. In order to do so, the following formulas are implemented:

$$\nu = \frac{{V_P}^2 - 2{V_S}^2}{2({V_P}^2 - {V_S}^2)} \qquad (4)$$

$$G = \rho {V_S}^2 \qquad (5)$$

$$E = 2G(1+\nu) \qquad (6)$$

Where ν is Poisson's ratio, G is Shear modulus , E is Young's modulus, ρ is density, V_P is P-wave velocity and V_S is Shear wave velocity. We can summarize the meaning of the different parameters as follows:

- Young's Modulus (E): A measure of the stiffness of a material. It describes the relationship between stress and strain in a material undergoing elastic deformation.
- Shear Modulus (G): A measure of a material's resistance to shear deformation.
- Poisson's Ratio (ν): A measure of the ratio of lateral strain to axial strain in a material subjected to axial stress.

Having the values of V_P and V_S from the retrieved models, by using these equations, mechanical parameters can be calculated. Needless to say that the value of density should be estimated. These parameters coupled with the ERT investigation result can lead to a better understanding of ground structure and the possible leakage positions.

4 Results

4.1 Electrical Resistivity Tomography Interpretation

4.1.1 Line ERT1

Figure 12 shows the 2-D inversion results of ERT survey for line ERT1 in dipole-dipole (a) and Wenner-Schlumberger configuration (b). Comparing these two figures, it can be noted that dipole-dipole configuration provides higher depth of investigation (nearly 60 m) while Wenner-Schlumberger survey reaches about half of it. In addition, the dipole-dipole arrangement is more sensitive to lateral resistivity changes, Wenner-Schlumberger, on the other hand, is more sensitive to vertical changes, as it can be seen in the figures.

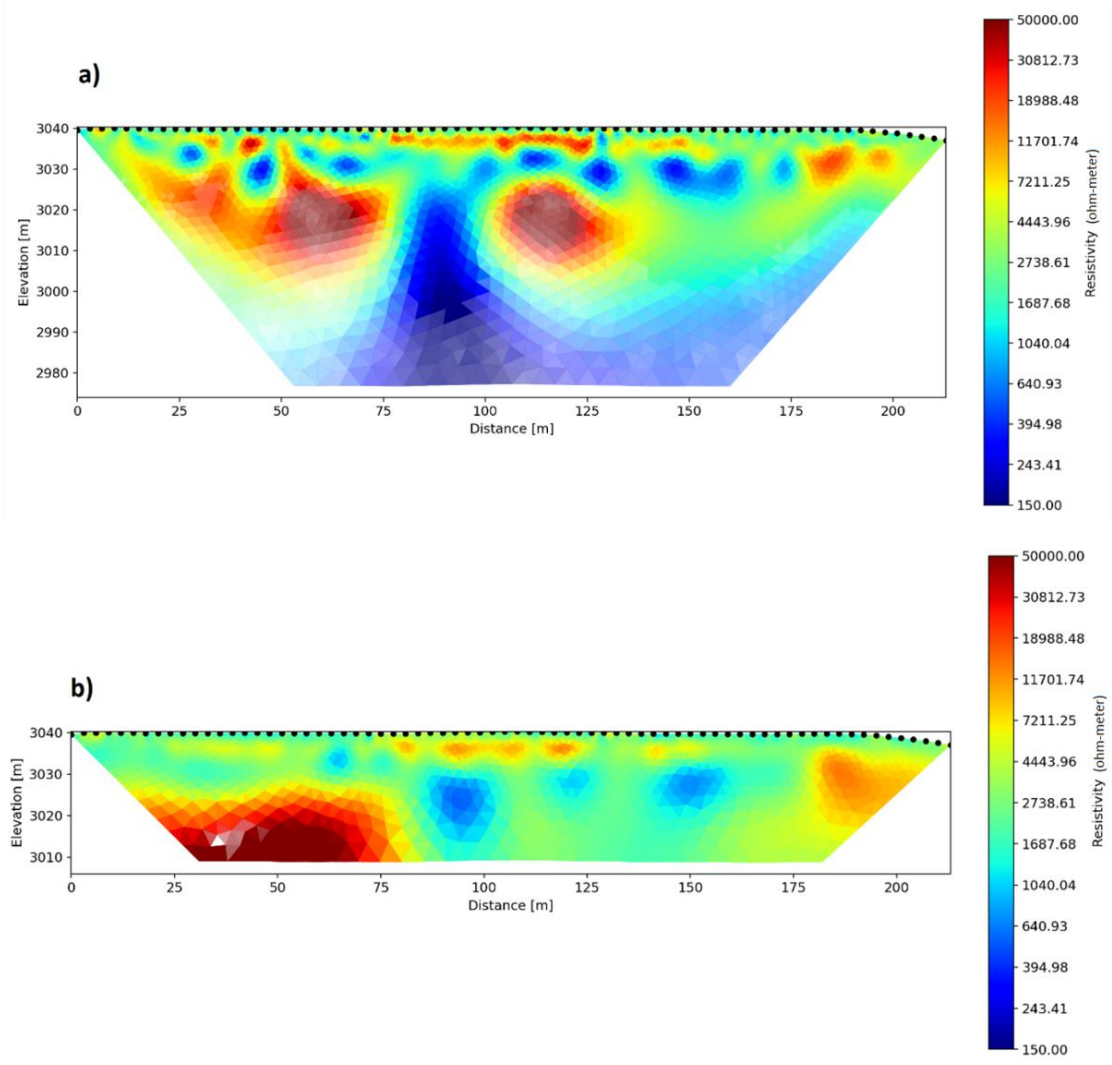

Figure 12: 2-D Inversion results of (ERT1) survey. (a) Dipole-Dipole (b) Wenner- Schlumberger array configuration.

In terms of potential leakage area, as mentioned before, generally, these areas are characterized by lower resistivity values compared to the surrounding dry or less saturated areas. So, we could expect the possible area of leakage to be located in the distance ranges between 75 to 100 meter from the beginning of the survey line ERT1 which is close to the drainage system of the basin, marked by a high resistivity anomaly.

4.1.2 Line ERT2

Figure 13, similarly, shows the 2-D inversion results of ERT survey for line ERT2 in dipole-dipole (a) and Wenner-Schlumberger configuration (b). Comparing them with the results of line ERT1 indicates that, overall, this line ERT2 is much more dryer and there might be no sign of leakage area.

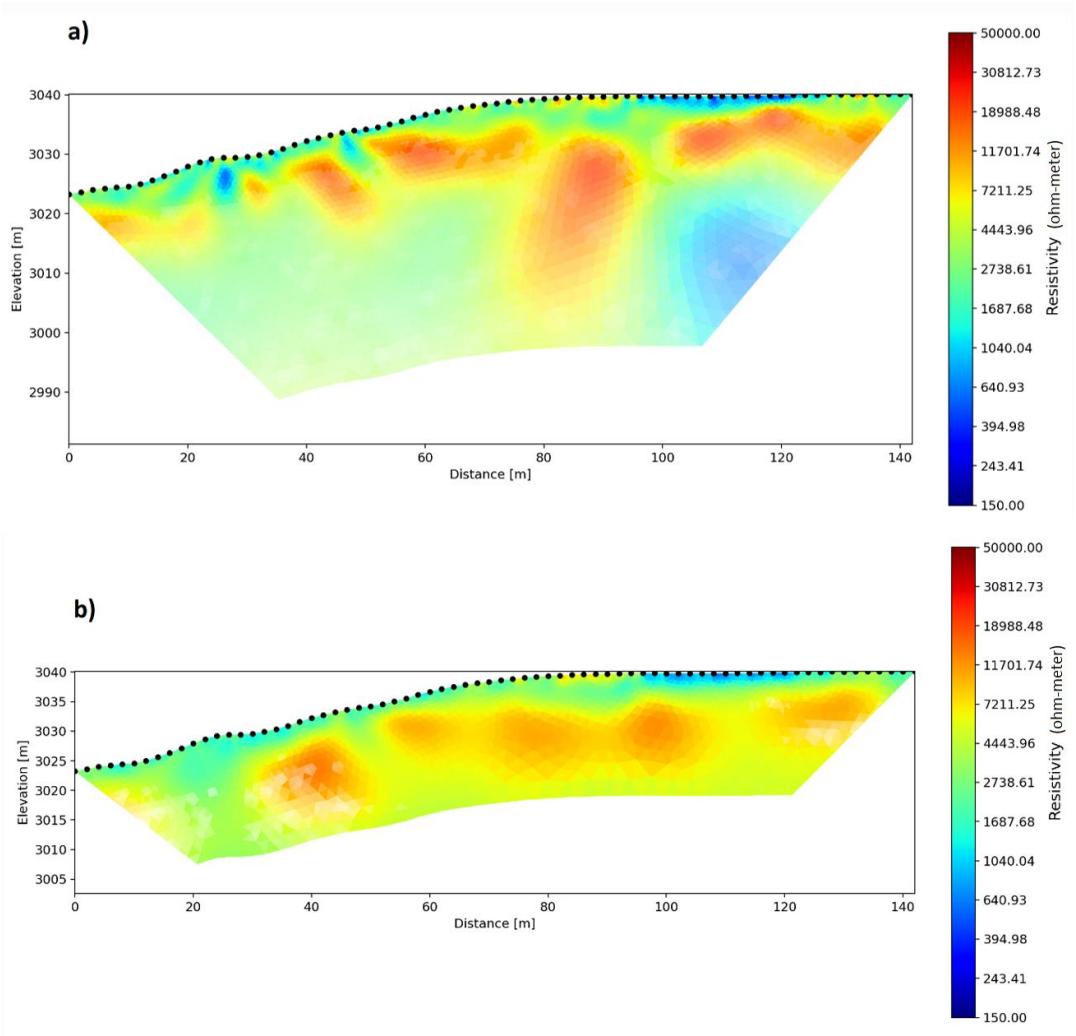

Figure 13: 2-D Inversion results of (ERT2) survey. (a) Dipole-Dipole (b) Wenner- Schlumberger array configuration.

As mentioned in chapter (3), the inversion process of ERT survey aims to minimize the difference between the observed apparent resistivity data and the simulated data from the forward model. This is done iteratively, updating the subsurface model in each iteration. Table (3) displays the total number of iterations and final misfit of ERT inversion results.

Table 3: Total number of iterations and final misfit (in percentage) of ERT inversion results.

LINE	CONFIGURATION	ITERATION	FINAL RMS MISFIT
ERT1	dd	3	1.16
	ws	3	1
ERT2	dd	6	1.06
	ws	5	1

It is clear from the Table 3 that the inversion method reaches acceptable results as we witnessed low values of Root Mean Squares for all four models. Low RMS values ensures reliable results of the inversion.

4.2 Seismic Refraction Tomography Interpretation

4.2.1 Line S1

As described in chapter 3, in the process of retrieving P-wave velocity model, firstly, first arrival travel times should be picked as an input data for inversion process. This picking process is carried out manually and the result can be seen in Figure 14 for all shots along the seismic line S1.

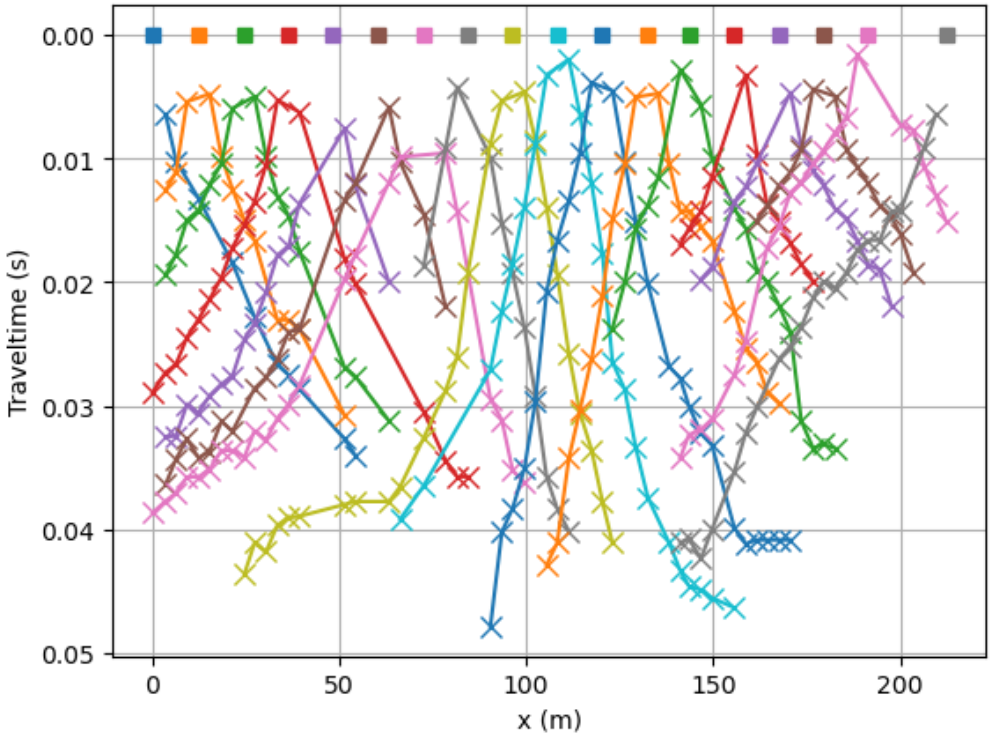

Figure 14: Manually-picked first arrival travel times of seismic refraction tomography for line S1.

It has been depicted in the Figure 14 that the smallest travel time values occurred exactly under each source, as departing from the sources, higher travel time values are recorded by further receivers. Figure 15 displays P-wave velocity model mesh grid (a) and Ray coverage and tracing plot (b) related to seismic line S1.

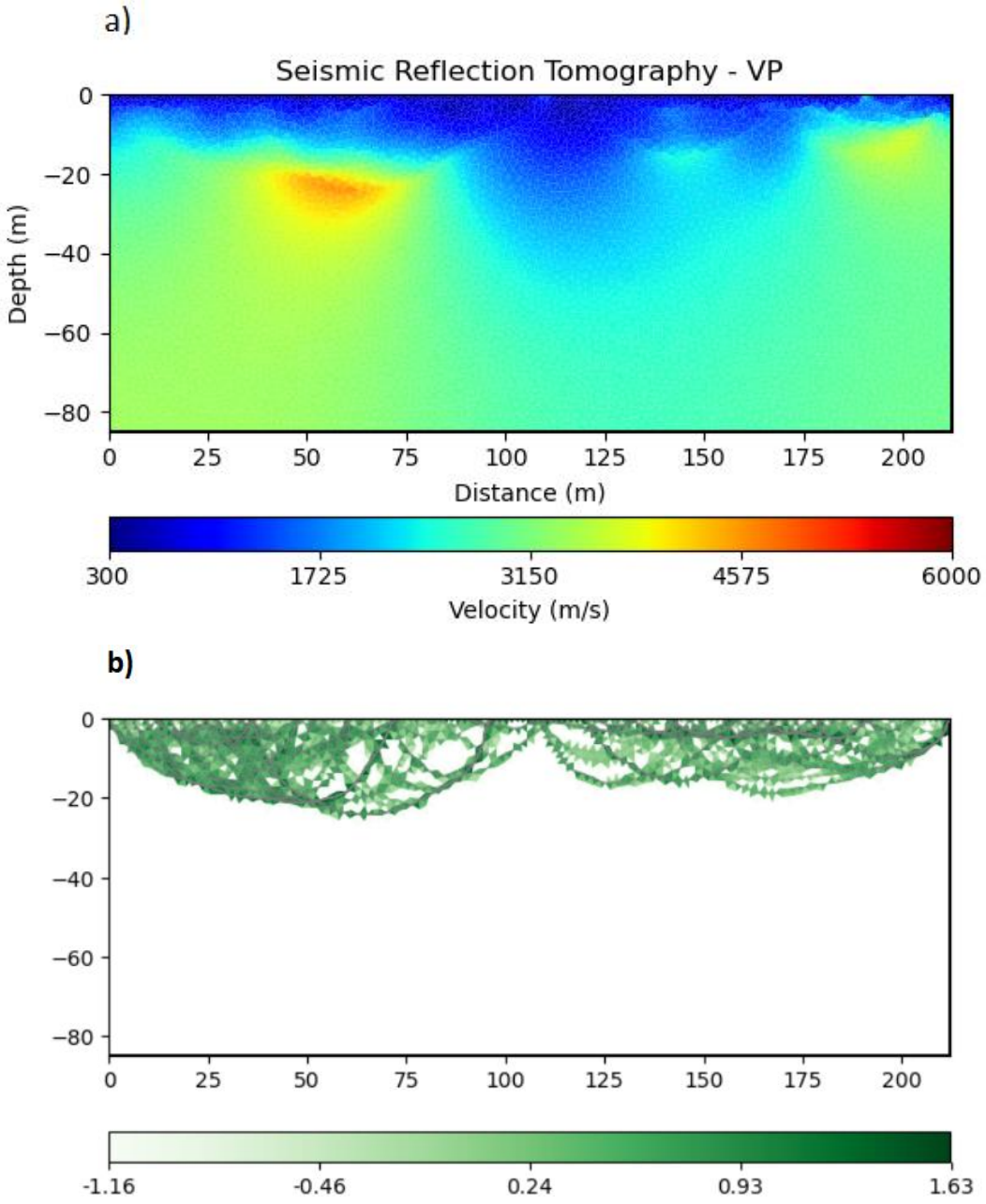

Figure 15: a) P-wave velocity model mesh grid. b) Ray coverage and tracing plot related to seismic line S1.

As described in chapter 3, the picked travel time data are used inside a Python library (PyGIMLi) to create P-wave velocity through the inversion process. Figure 15(a) shows the velocity model which is retrieved by interpolating of mesh-grid elements of line S1. As it is clear, this plot does not show much information in deeper parts, the reason is the fact that not all elements of the mesh-grid have been investigated by the seismic waves. So, the investigated area has to be restricted by seismic ray coverage. Figure 15(b) shows the seismic ray coverage. It can be perceived that the ray coverage only reaches to approximately 20 meters of depth. Figure 16 displays the final P-wave velocity model after applying the coverage limit.

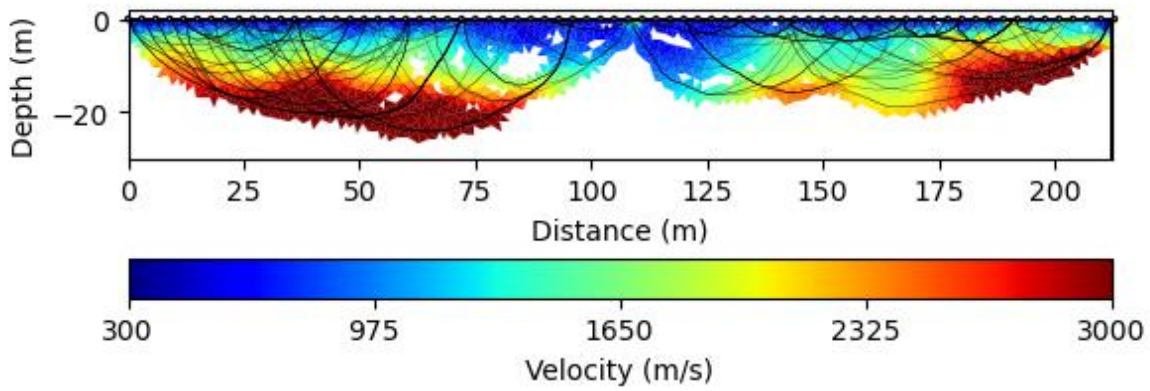

Figure 16: final P-wave velocity model for line S1.

Referring to Figure 16, the area of higher velocity values might indicate the presence of dense and high-consolidated material (e.g. bedrock or big rock blocks), while lower velocity values might represent the un-consolidated sediment or possibly water saturated material inside the embankment.

4.2.2 Line S2

Figure 17 shows the plot of first arrival times for seismic refraction analysis related to all the shots of line S1. Again, distancing from the sources for each shot, an increasing trend in first arrival travel times can be witnessed on the graph.

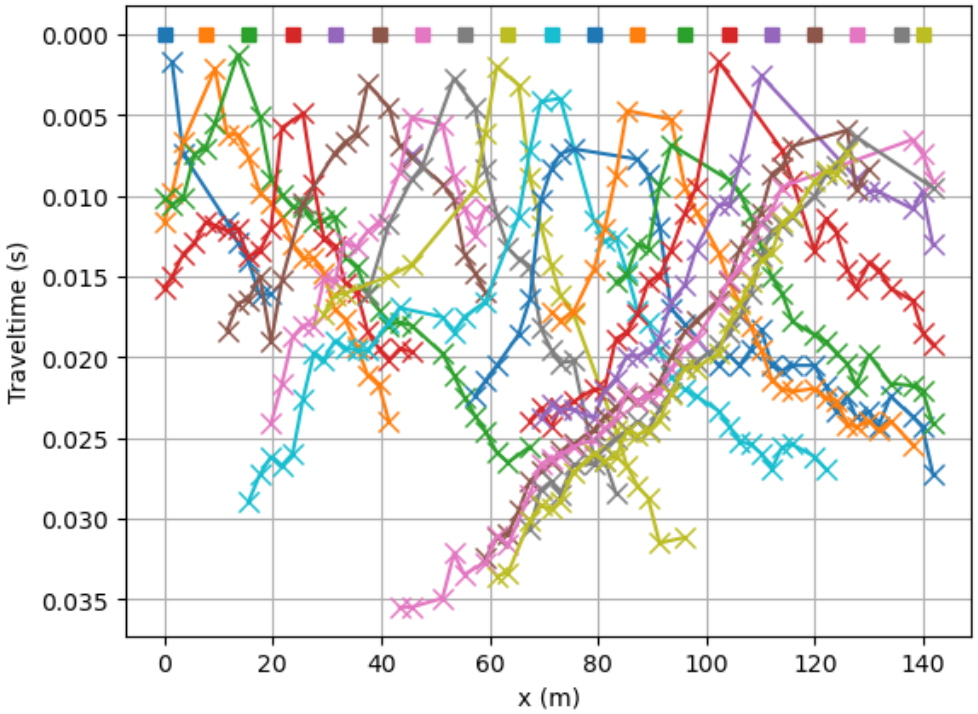

Figure 17: Manually-picked first arrival travel times of seismic refraction tomography for line S2.

Figure 18(a) shows the velocity model which is retrieved by interpolating of mesh-grid elements of line S2. The similar discussion to line S1 could be mention also for line S2 in terms of mesh-grid velocity model, ray-coverage plot and final P-wave velocity model limited by ray traces which is shown respectively in Figure 18(a), (b) and (c). The seismic ray traces for line S2 also reaches about 20 meters in depth similar to line S1. Concerning P-wave velocity model interpretation, comparing line S1 and line S2, consistent with the ERT results, as line S2 shows higher velocity values, it might represent much more dryer material than line S2.

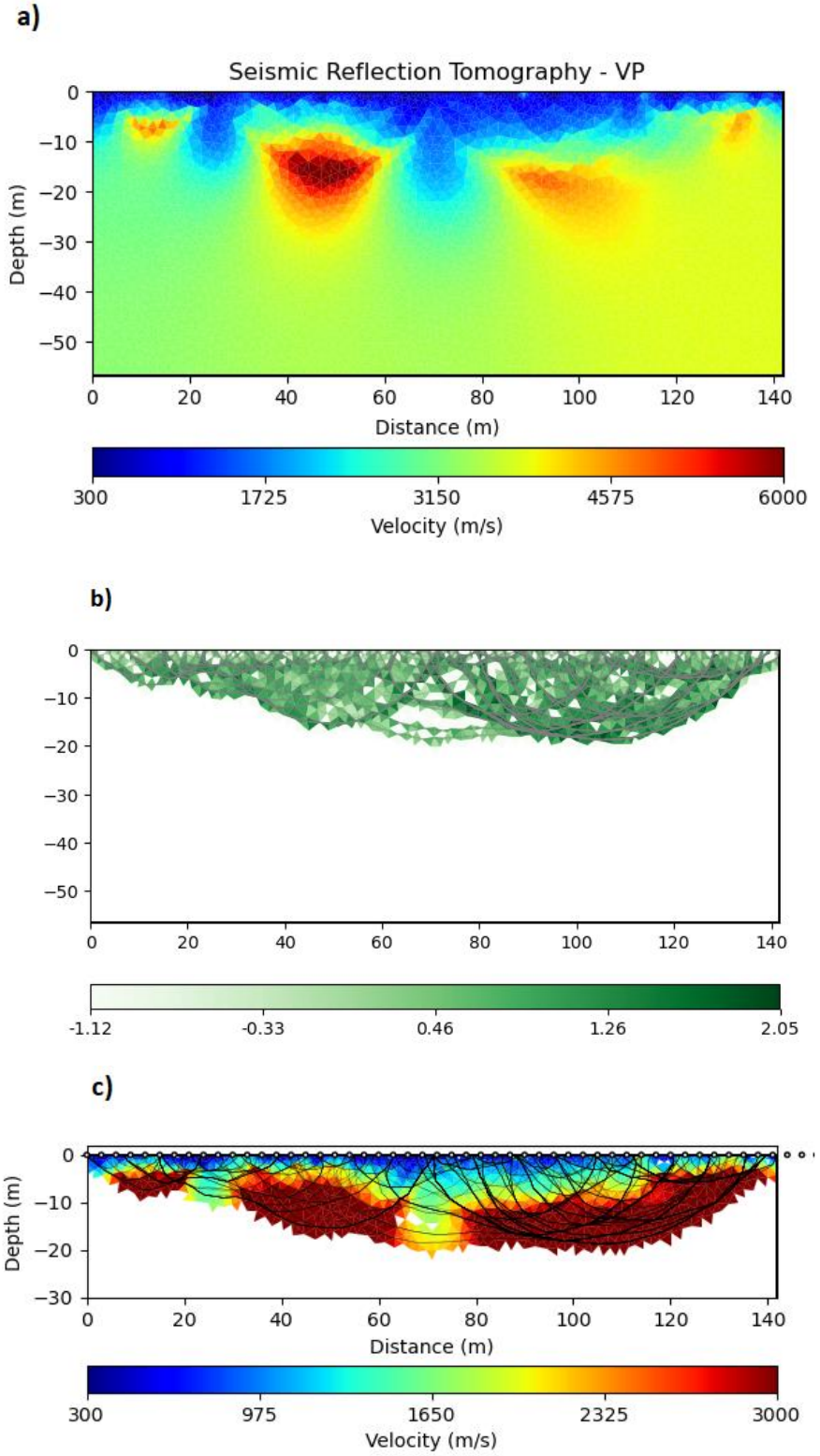

Figure 18: a) P-wave velocity model mesh grid. b) Ray coverage and tracing plot. c) final P-wave velocity model related to seismic line S2.

4.3 Surface Wave Analysis

4.3.1 Dispersion Curves

As mentioned in chapter 3, in order to retrieve shear-wave velocity model, firstly, dispersion curve is needed to be generated through picking fundamental mode from each spectra which process is discussed before. This procedure has been done with the help of some Matlab codes. Figure 19 shows the final selected dispersion curves in wavelength-phase velocity plots for (a): line S1 and (b): line S2.

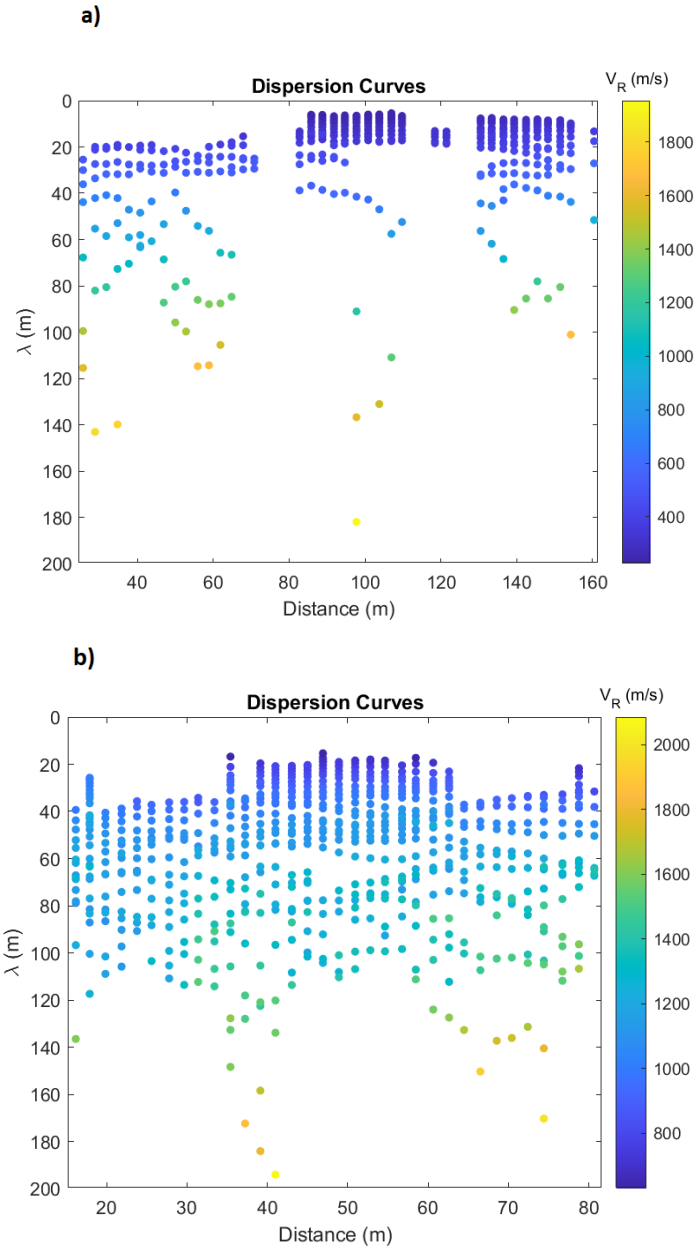

Figure 19: Final dispersion curve of Rayleigh wave velocity for a) line S1 and b) line S2.

According to Figure (19), clearly, every point in dispersion curves represents Rayleigh wave velocity (V_R) and the corresponding wavelength (λ). It also can be perceived that dispersion curve related to the line S2 covers more area due to the fact that more fundamental mode curves could be extracted from spectra all over the line S1 compared to line S2. Due to data quality, indeed, no dispersion curves were retrieved along line S2 after a distance of 80 m from the line start.. These selected dispersion curves should be modelled in the inversion process which, again, is done by Matlab codes. Exemplificative results of the fitting are shown in Figure 20.

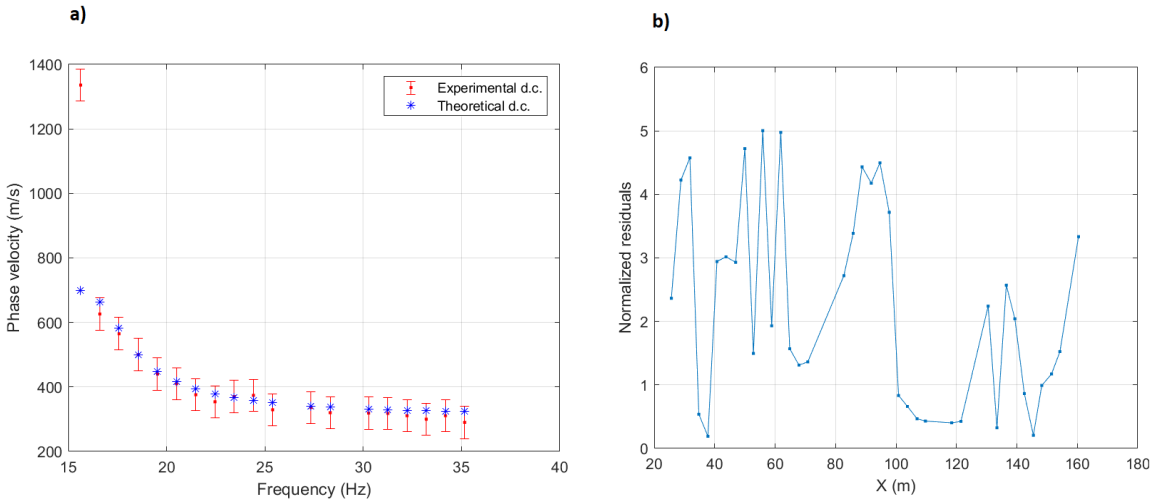

Figure 20: a)The results of fitting process between experimental and theoretical dispersion curves. b) The simulation misfit graph.

Figure 20 indicates an examples of the fitting dispersion curve simulation(a), and the final simulation misfit graph (b) along the line. The computed dispersion curve shows a decent fitting which depicts satisfying simulation, particularly, in higher frequencies. Dispersion curve simulations coupled with an initial shear wave velocity model would generate the final shear wave velocity model which is an iterative process done by Matlab codes. The initial model is created based on prior geological knowledge and the model would be updated after each iteration. The results are shown in Figure 21.

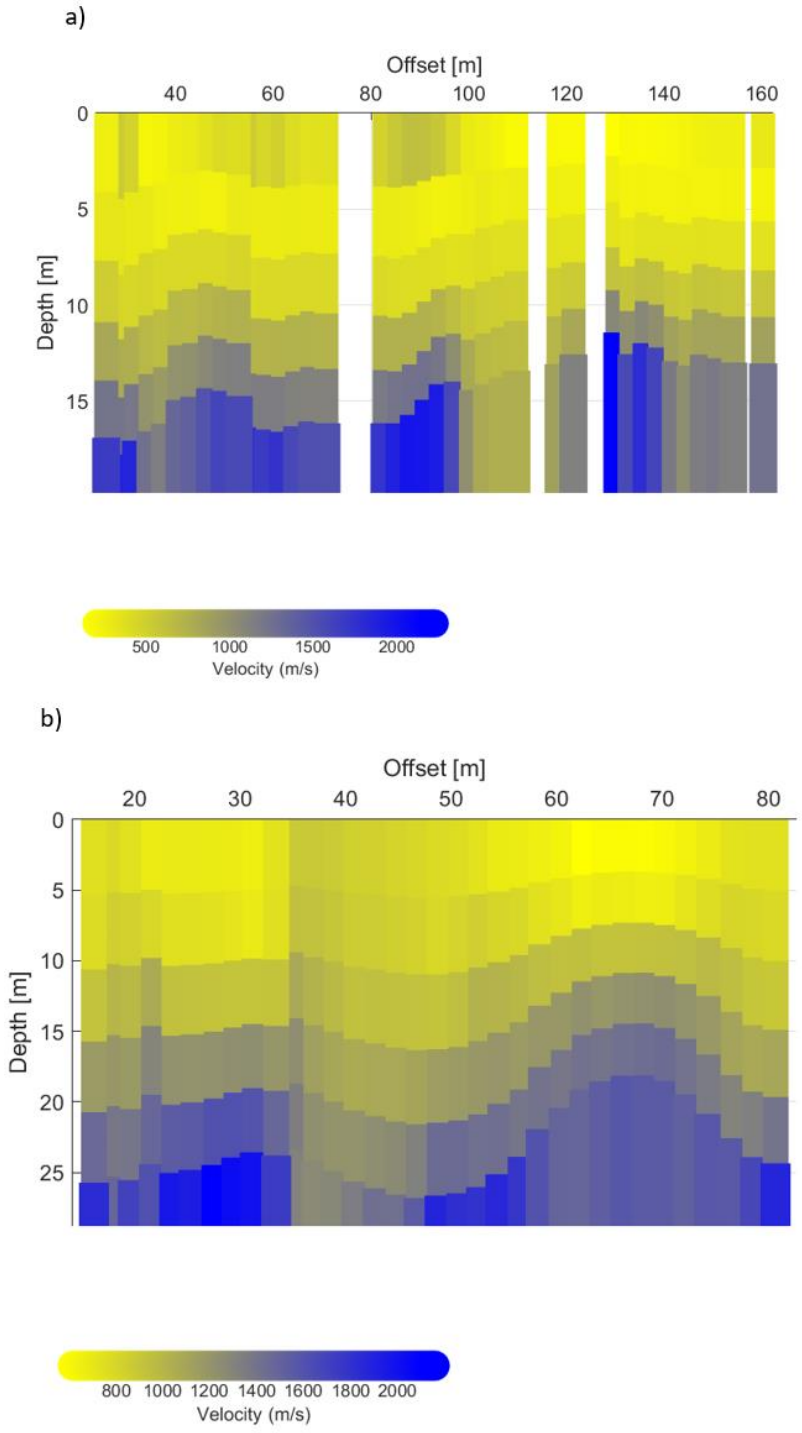

Figure 21: The final shear wave velocity model for seismic line S1 and S2.

Figure 21 shows the final result of shear wave velocity modelling for line S1 and S2 which are retrieved after 39 iteration. The models depict approximately good lateral and vertical velocity variation. As already noticed in the electrical results, also the shear wave velocity variations appear more marked along S1, while S2 variations are smoother.

4.3.2 Mechanical Parameters

As discussed before, the seismic survey is carried out together with surface wave analysis in order to achieve mechanical properties of the underlying ground to be assessed. To do so, firstly, shear wave velocity model is needed to be interpolated inside the P-wave velocity mesh-grid. Again, Matlab codes are implemented in order to fulfil this goal. Results can be seen in Figure 22 and 23 for line S1 and S2, respectively.

As it can be perceived from Figure 22 and 23, shear wave velocity is successfully interpolated into the P-wave velocity mesh and it is ready for the next step which is computing the Poisson's ratio, Young's modulus and Shear modulus for each cell in the mesh-grid. The final results can be seen in Figure 24 and Figure 25 for two different modes: a) Ray-coverage mesh-grid b) interpolating mesh-grid. The white cells indicates the fact that there is no data to be plotted for these parts.

According to Figure 24 and 25, the Poisson's ratio shows variability along the line S1 and S2. It can be discussed that the area of low Poisson's ratio values (below 0.3) which corresponds to high value of Young's modulus and Shear modulus, could indicate very compact material which might be not saturated. In contrary, higher Poisson's ratio values could be interpreted as a sign of weak and saturated material. The wide gap in Figure 25 is due to the fact that there has been no possibility to extract dispersion curve from the length of 80 m onward for the line S2 which could affect the result quality.

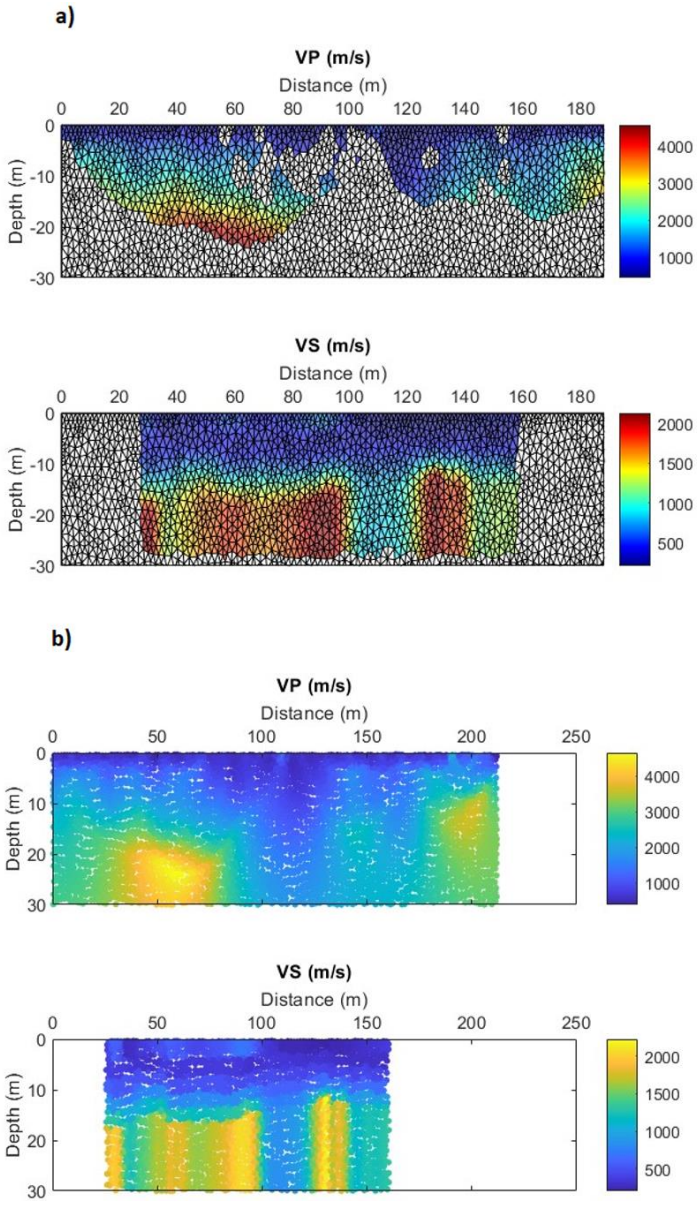

Figure 22: P-wave velocity model and interpolated Shear wave velocity model for seismic lineS1 plotted on (a): mesh elements having coverage > 1 and (b): central points of all the mesh elements (interpolated where data coverage is not available).

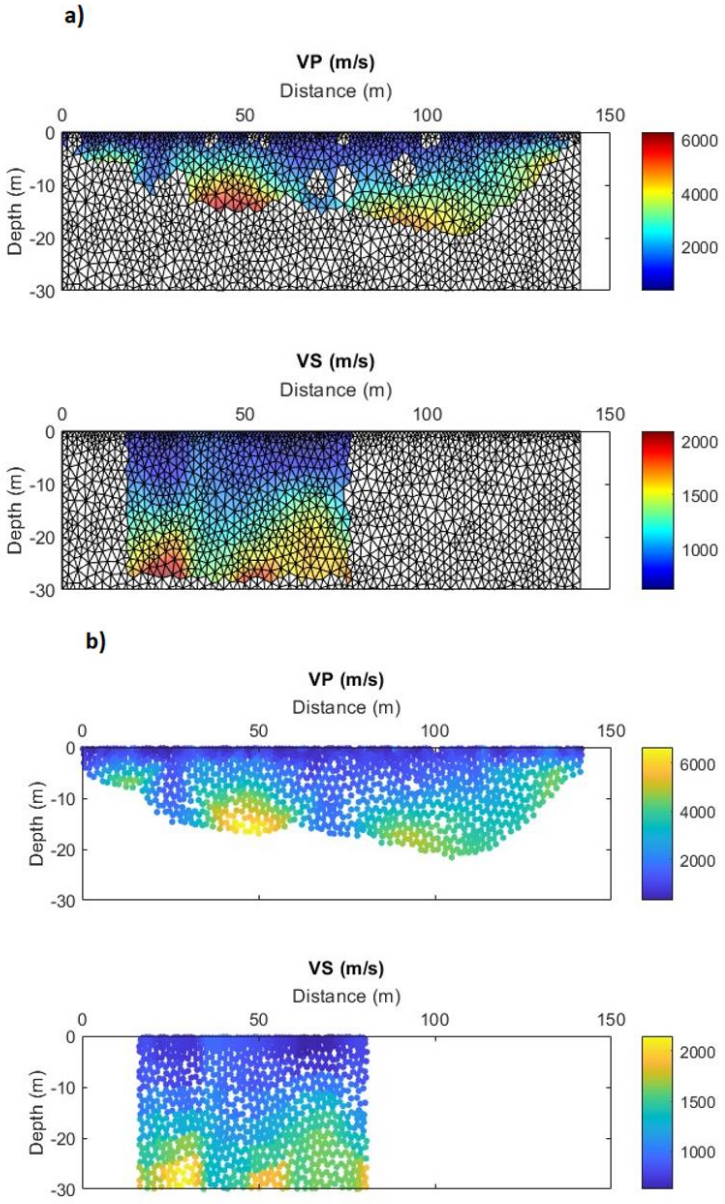

Figure 23: P-wave velocity model and interpolated Shear wave velocity model for seismic lineS2 based on (a): ray-coverage mode and (b): mesh-grid mode.

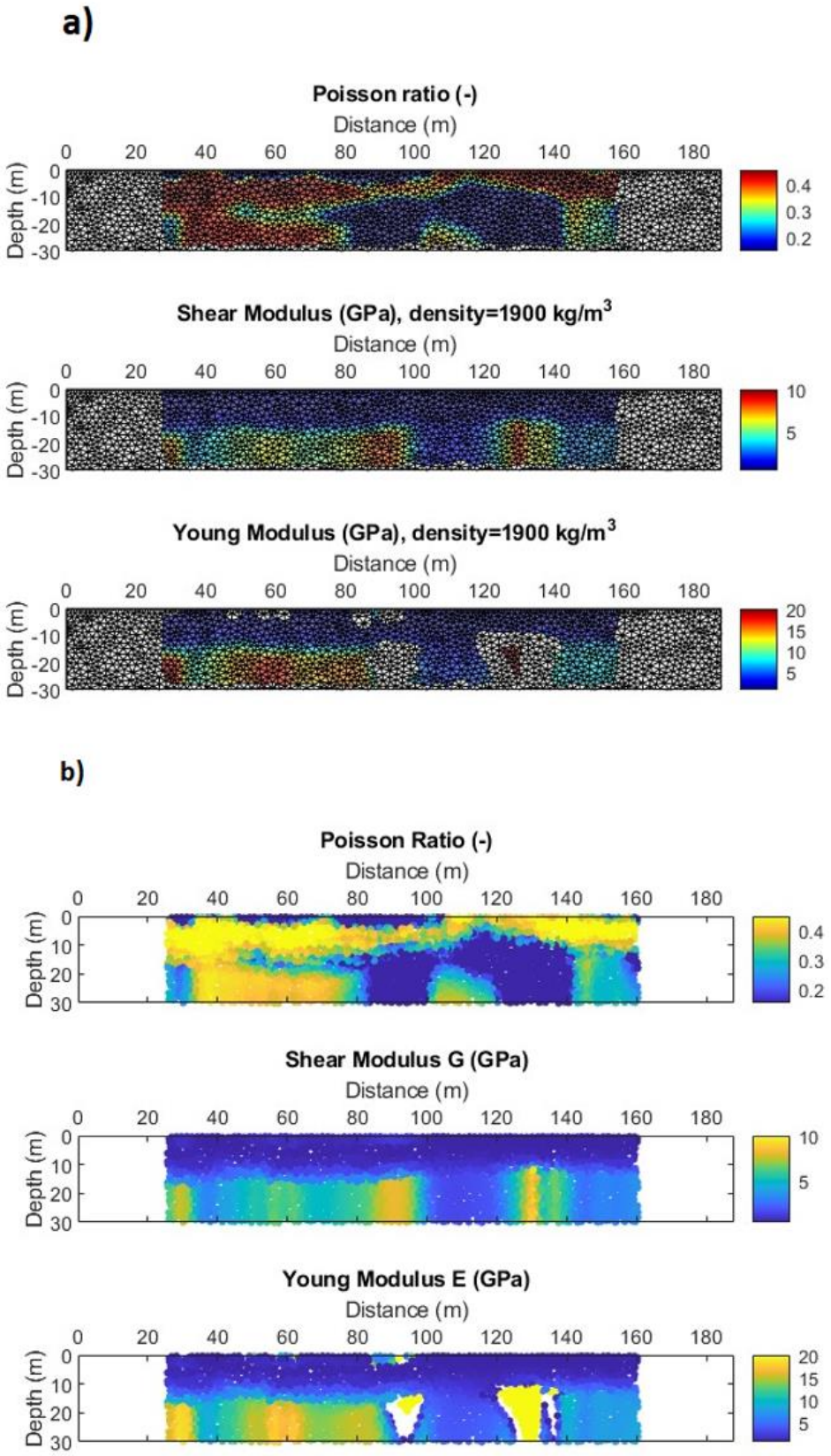

Figure 24: Mechanical parameters mesh-grid for line S1 in a) Ray-coverage b) Interpolation mode.

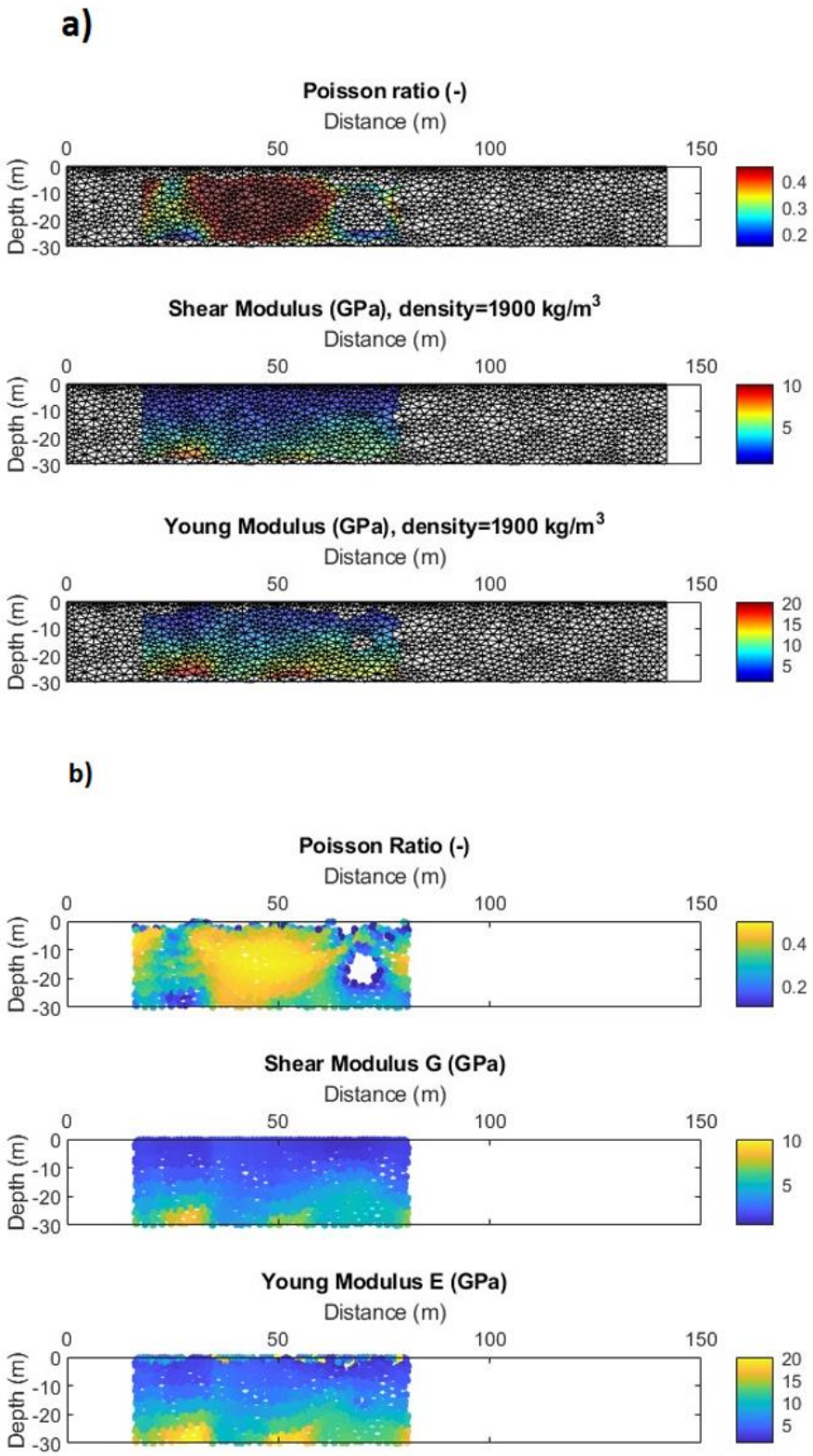

Figure 25: Mechanical parameters mesh-grid for line S2 in a) Ray-coverage b) Interpolation mode.

4.3.3 Results Comparison

Figure 26 and 27 show the comparison between ERT investigation and mechanical parameters to better understand the internal structural setting of the embankments along line S1 and S2.

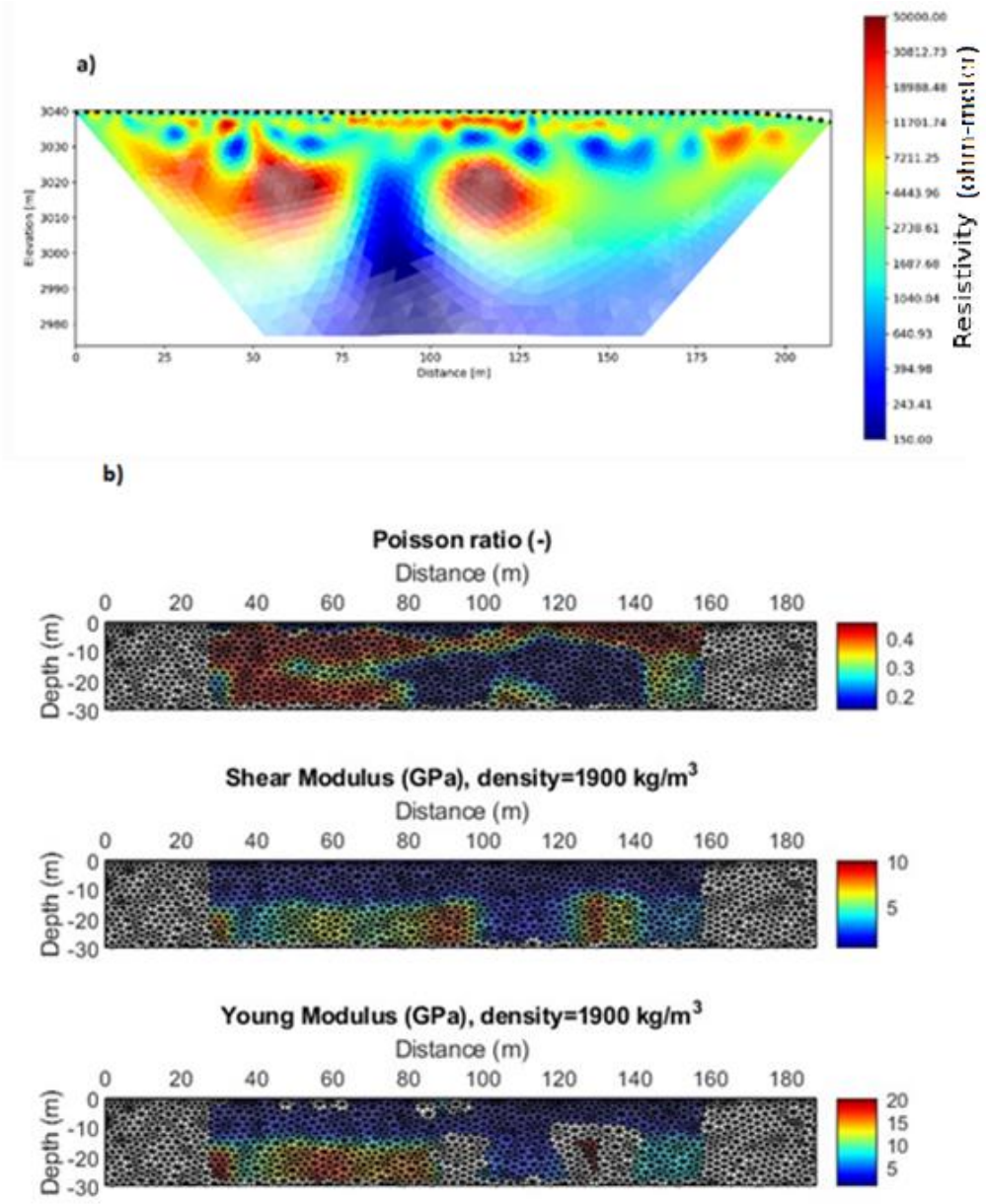

Figure 26: Comparison between: a)ERT investigation and b)mechanical parameters modelling results for line S1.

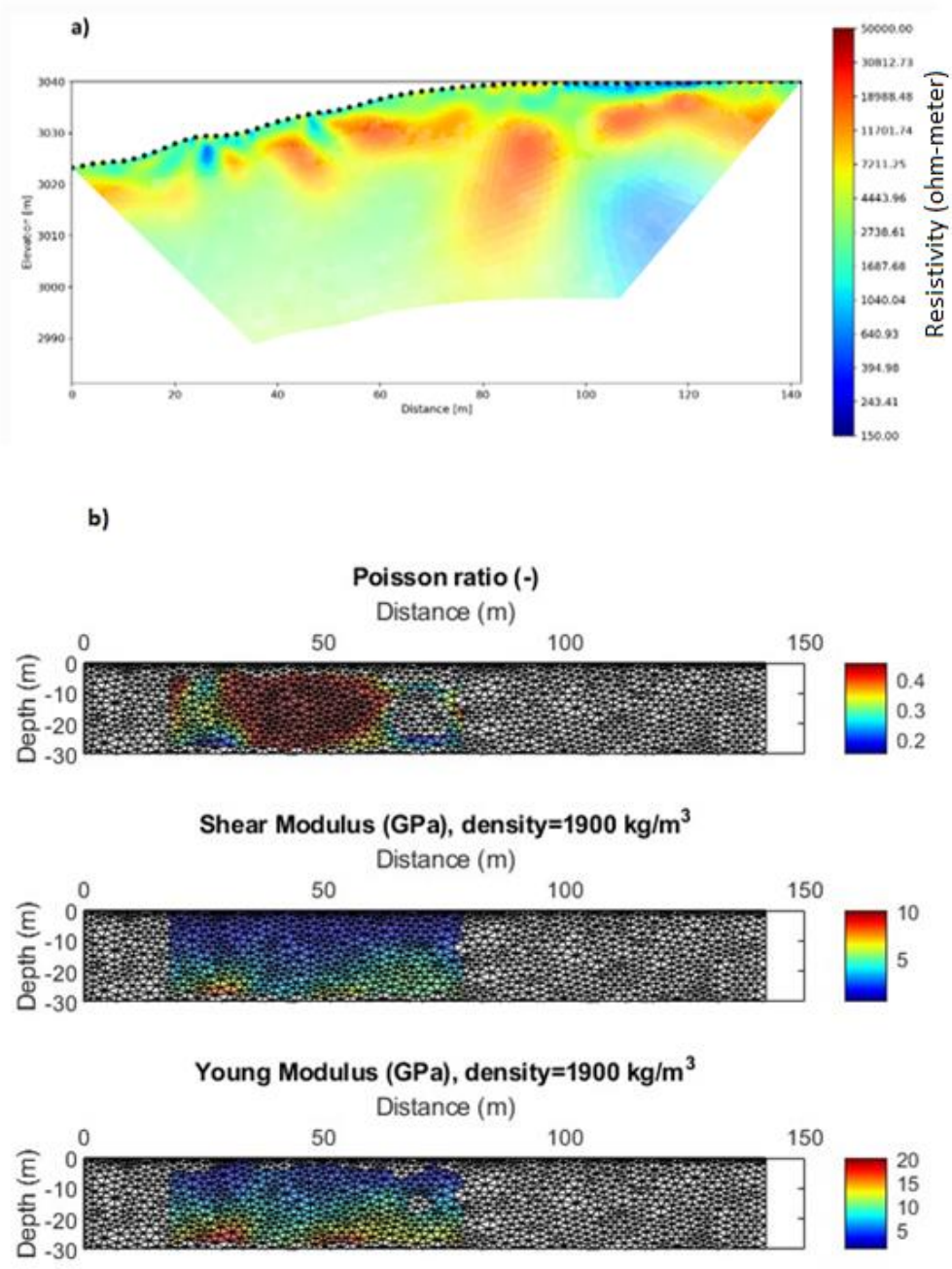

Figure 27: Comparison between: a)ERT investigation and b)mechanical parameters modelling results for line S2.

4.3.3.1 Saturation Analysis

Along Line 1, the results indicate a very thin surface layer with material resistivity higher than 10,000 ohm-meters, which can be seen in Figure 26(a), suggesting unsaturated conditions. Beneath this, a second layer exhibits potentially higher water content, indicated by lower resistivity values (in blue). At depths exceeding 20 meters, significant resistivity anomalies are observed. The first high-resistivity anomaly, located between 50 and 75 meters, lacks corroborating evidence from the site. It may correspond to a concrete structure, large boulders, or intact bedrock. The second anomaly, found between 100 and 150 meters, is likely related to an empty drainage canal of the lake, as visible in aerial photographs of the site. The most notable anomaly, between 75 and 100 meters, potentially indicates seepage near the drainage system.

Comparing the electrical resistivity tomography of Line 2 with Line 1 reveals that Line 2 does not show anomalies with high resistivity contrasts along the investigated section. The first shallow layer in line 2 exhibits intermediate resistivity values, followed by a layer of higher resistivity values within the embankment, indicating more compacted or less saturated material compared to Line 1.

4.3.3.2 Mechanical Analysis

Mechanically, these anomalies are associated with reductions in shear modulus and Young's modulus (green areas). The Poisson's ratio analysis shows that shallow materials (red areas in the resistivity tomography) exhibit low Poisson's ratios, indicating a lack of saturation. Conversely, the second layer has a very high Poisson's ratio, confirming potential saturation. Interpretation of the Poisson's ratio at depths of 20 to 30 meters is challenging due to significant variability, which may be attributed to either saturation or material weakness. It is also worth to mention that the seismic survey results could assure only up to the depth of 30 meters. The material could have different saturation in higher depth as it is reported in ERT results.

Unfortunately, the shear velocity model of line 2, was only retrievable for a small portion of 80 meters, resulting in uncertain and potentially overestimated Poisson's ratio values, which are not considered reliable. Additionally, the shear wave velocity model is too limited to provide meaningful information.

5 Conclusion

In this study, Electrical Resistivity Tomography (ERT), Seismic Refraction Survey and Surface Wave Analysis were performed along two survey lines in the embankments of an artificial water basin to investigate potential seepage. The results from ERT indicated that varying saturation levels were present within the embankment materials. Specifically, along Line S1, a potential anomaly characterized by higher saturation levels was identified between 75 to 100 meters. This anomaly is situated near a high resistivity region, which is likely associated with the lake's drainage system. In contrast, the material along the second survey line appeared more homogeneous, indicating no significant anomalies. The seismic analysis provided estimations of the mechanical parameters of the embankment materials. These parameters, combined with the ERT data, offered a comprehensive understanding of the subsurface conditions and potential seepage pathways. It is suggested that the combination of ERT and seismic methods is effective for detecting potential leakage in artificial water basins. The following recommendations are proposed to enhance future surveys which might help in decision making process and mitigation steps to be taken:

- Increased Survey Density: A higher density of survey lines could be implemented to provide a more detailed subsurface image, improving the detection and characterization of seepage pathways.

- Longer Survey Lines: Extending the length of the survey lines may capture a broader area, potentially identifying additional anomalies or confirming the extent of detected ones.

- Integration with other Geophysical Methods: ERT and seismic methods could be combined with other geophysical techniques, such as Ground Penetrating Radar (GPR), to enhance the accuracy and reliability of the results.

- Time-lapse Surveys: Surveys could be conducted during different seasons to help in understanding the temporal variations in saturation and the impact of seasonal

changes on seepage patterns. It could also help to monitor the progression of seepage and the effectiveness of possible mitigation efforts.

- Advanced Data Processing Techniques: More sophisticated data processing and inversion techniques could be utilized to improve the resolution and interpretability of the geophysical data.

- Modelling hydrogeological situation of the site to better comprehend the expected ground structure.

In conclusion, the integrated approach of ERT and seismic methods demonstrated in this study to provide a robust framework for the detection and analysis of seepage in artificial water basins. These findings can inform maintenance strategies and the design of more effective monitoring systems for such critical infrastructure.

References

Adamo, Nasrat, Al-Ansari, Nadhir, Sissakian, Varoujan, Laue, Jan, & Knutsson, Sven. (2020). Geophysical Methods and their Applications in Dam Safety Monitoring. *Journal of Earth Sciences and Geotechnical Engineering, 11,* 291-345.

Aki, K., & Richards, P. G. (2002). *Quantitative seismology.* University Science Books.

Alsadi, H., & Baban, E. (2020). Introduction to seismic exploration.

Auken, E., et al. (2015). An integrated processing scheme for high-resolution airborne electromagnetic surveys, the SkyTEM system. *Exploration Geophysics.*

Binley, A., & Kemna, A. (2005). DC resistivity and induced polarization methods. In Y. Rubin & S. S. Hubbard (Eds.), *Hydrogeophysics.* Springer.

Blanchy, G., Nguyen, F., Kemna, A., & Robert, T. (2020). ResIPy, an intuitive open-source software for complex geoelectrical inversion/modeling. *Journal of Open Source Software, 5*(46), 2006.

Butler, D. K., et al. (2012). Geophysical Methods for Subsurface Characterization. In *Geotechnical and Environmental Geophysics (Vol. 2).* SEG Books.

Cardarelli, E., & De Donno, G. (2019). Advances in electric resistivity tomography: Theory and case studies. In R. Persico, S. Piro, & N. Linford (Eds.), *Innovation in near-surface geophysics* (pp. 23–57). Elsevier.

Chambers, J. E., et al. (2002). Electrical resistivity tomography applied to geologic, hydrogeologic, and engineering investigations at a former waste-disposal site. *Geophysics.*

Chambers, J. E., et al. (2014). 4D electrical resistivity tomography monitoring of soil moisture dynamics in an operational railway embankment. *Near Surface Geophysics, 12*(1), 61-72.

Dziewonski, A. M., & Anderson, D. L. (1981). Preliminary Reference Earth Model (PREM). *Physics of the Earth and Planetary Interiors, 25*(4), 297-356.

Fischer, A., Olefs, M., & Abermann, J. (2012). Glaciers, Water and Ecosystem Services in the Austrian Alps. *Hydrological Processes, 26*(12), 2067-2078.

Foti, S., Lai, C. G., Rix, G. J., & Strobbia, C. (2014). Surface wave methods for near-surface site characterization. CRC Press.

Hanzer, F., Förster, K., Nemec, J., & Strasser, U. (2018). Projected Snowmaking Potential and Future Climate in Alpine Ski Resorts. *Water Resources Research, 54*(2), 932-950.

Herrmann, R. B. (2013). Computer programs in seismology: An overview of synthetic seismogram computation. *Saint Louis University.*

Johansson, S., & Dahlin, T. (2002). Seepage monitoring in an earth embankment dam by repeated resistivity surveys. *Geophysical Prospecting, 50*(3), 109-120.

Kearey, P., Brooks, M., & Hill, I. (2013). *An Introduction to Geophysical Exploration (3rd ed.).* Wiley.

Lagoe, M. B., Kovach, R. L., Roberts, R. G., & Swift, S. (1979). Application of seismic reflection methods to dam safety investigations. *Journal of the Geotechnical Engineering Division, 105*(12), 1427-1445.

Lay, T., & Wallace, T. C. (1995). *Modern global seismology.* Academic Press.

Lin, C., Lin, C. H., Hung, Y., Chung, C., Wu, P., & Liu, H. (2018). Application of geophysical methods in a dam project: Life cycle perspective and Taiwan experience. *Journal of Applied Geophysics, 158,* 82-92.

Loke, M. H. (2020). Tutorial: 2-D and 3-D electrical imaging surveys. *Geotomosoft Solutions, Malaysia.*

Loke, M. H., & Barker, R. D. (1996). Rapid least-squares inversion of apparent resistivity pseudosections by a quasi-Newton method. *Geophysical Prospecting, 44*(1), 131-152.

Loke, M. H., et al. (2013). Recent developments in the direct-current geoelectrical imaging method. *Journal of Applied Geophysics.*

Menke, W. (1989). *Geophysical Data Analysis: Discrete Inverse Theory.* Academic Press.

Nolet, G. (1987). *Seismic tomography: With applications in global seismology and exploration geophysics.* Springer.

Nguyen, F., & Kemna, A. (2020). An overview of ResIPy: A Python-based framework for geoelectrical inversion and modeling. *Computers & Geosciences, 135,* 104379.

Pogliotti, P., Guglielmin, M., Cremonese, E., Morra di Cella, U., Filippa, G., Pellet, C., & Hauck, C. (2015). Warming permafrost and active layer variability at Cime Bianche, Western European Alps. *The Cryosphere, 9,* 647–661.

Redpath, B. B. (1973). Seismic refraction exploration for engineering site investigations (Technical Report E-73-4). *U.S. Army Engineer Waterways Experiment Station.*

Reynolds, J. M. (2011). *An Introduction to Applied and Environmental Geophysics (2nd ed.).* Wiley.

Rixen, C., Teich, M., Lardelli, C., Gallati, D., Pohl, M., Pütz, M., & Bebi, P. (2011). Winter Tourism and Climate Change in the Alps: An Assessment of Resource Consumption, Snow Reliability, and Future Snowmaking Potential. *Mountain Research and Development, 31*(3), 229-236.

Schrott, L., & Sass, O. (2008). Application of Field Geophysics in Geomorphology: Advances and Limitations Exemplified by Case Studies. *Geomorphology, 93*(1-2), 55-73.

Sjogren, B. (1984). *Shallow refraction seismic (1st ed.).* Chapman and Hall Ltd.

Soupios, P. M., Papazachos, C. B., Sarris, A., Papazachou, O., Vargemezis, G., & Vallianatos, F. (2007). Application of electrical resistivity tomography in a landslide investigation in Greece. *Journal of Geophysics and Engineering, 4*(3), 242-253.

Steiger, R., & Mayer, M. (2008). Snowmaking and Climate Change: Future Options for Snow Production in Tyrolean Ski Resorts. *Mountain Research and Development, 28*(3/4), 292-298.

Stein, S., & Wysession, M. (2003). *An introduction to seismology, earthquakes, and earth structure.* Wiley-Blackwell.

Stein, S., & Wysession, M. (2009). *An introduction to seismology, earthquakes, and earth structure.* John Wiley & Sons.

Telford, W. M., Geldart, L. P., Sheriff, R. E., & Keys, D. A. (1990). *Applied geophysics (2nd ed.).* Cambridge University Press.

USBR. (1960). Seismic methods in dam safety investigations. *Technical Memorandum No. 821. United States Bureau of Reclamation.*

Van Norstrand, R. G., & Cook, L. (1966). Interpretation of Resistivity Data. *Geological Survey Professional Paper, p.16. Washington.*

Ward, S. H. (1990). *Geotechnical and Environmental Geophysics: Volume I, Review and Tutorial.* Society of Exploration Geophysicists.